1 **Quantification of hydraulic trait control on plant hydrodynamics and risk of hydraulic**

2 **failure within a demographic structured vegetation model in a tropical forest (FATES-**

3 **HYDRO V1.0)**

4 Chonggang Xu[1], Bradley Christoffersen[2], Zachary Robbins[1], Ryan Knox[3], Rosie A. Fisher[4],

5 Rutuja Chitra-Tarak[1], Martijn Slot[5], Kurt Solander[1], Lara Kueppers[3,6], Charles Koven[3], Nate

6 McDowell[7,8]

7 1: Earth and Environmental Sciences Division, Los Alamos National Laboratory, Los Alamos

8 NM, USA

9 2: School of ~~Integrated~~Integrative Biological and Chemical Sciences, University of Texas Rio

10 Grande Valley, TX, USA

11 3: Lawrence Berkeley National Laboratory, Berkeley, CA USA

12 4. CICERO Centre for International Climate Research, Oslo, Norway

13 5: Smithsonian Tropical Research Institute, Apartado 0843-03092, Balboa, Ancon, Republic of

14 Panama

15 6: Energy and Resources Group, University of California, Berkeley, CA USA

16 7: Atmospheric Sciences and Global Change Division, Pacific Northwest National Laboratory,

17 Richland, WA, USA

18 8: School of Biological Sciences, Washington State University, Pullman, WA, USA

23 Corresponding author: Chonggang Xu (cxu@lanl.gov)

Abstract: Vegetation plays a key role in the global carbon cycle and thus is an important component within Earth system models (ESMs) that project future climate. Many ESMs are adopting methods to resolve plant size and ecosystem disturbance history using vegetation demographic models. These models make it feasible to conduct more realistic simulation of processes that control vegetation dynamics. Meanwhile, increasing understanding of the processes governing plant water use, and ecosystem responses to drought in particular, has led to the adoption of dynamic plant water transport (i.e., hydrodynamic) schemes within ESMs. However, the impact of plant hydraulic trait variation in trait-diverse tropical forests is understudied. In this study, we report on a sensitivity analysis of an existing hydrodynamics (HYDRO) model that is updated and incorporated into the Functionally Assembled Terrestrial Ecosystem simulator (FATES). The size and canopy structured representation within FATES is able to simulate how plant size and hydraulic traits affect vegetation dynamics and carbon/water fluxes. To better understand this new model system and its functionality in tropical forest systems in particular, we conducted a global parameter sensitivity analysis at Barro Colorado Island, Panama. We assembled 942 observations of plant hydraulic traits on 306 tropical plant species for stomata, leaves, stems, and roots, and determined the best-fit statistical distribution for each trait, which was used in model parameter sampling to assess the parametric sensitivity. We showed that, for simulated leaf water potential and loss of hydraulic conductivity across different plant organs, the four most important traits were associated with xylem conduit taper (buffers increasing hydraulic resistance with tree height), stomatal sensitivity to leaf water potential, maximum stem hydraulic conductivity, and the partitioning of total hydraulic resistance above vs. belowground. Our analysis of individual ensemble members revealed that trees at a high risk of hydraulic failure and potential tree mortality generally have higher conduit taper, maximum xylem conductivity, stomatal sensitivity to leaf

48 water potential, and lower resistance to xylem embolism for stem and transporting roots. We

49 expect that our results will provide guidance on future modeling studies using plant hydrodynamic

50 models to predict the forest responses to droughts, and future field campaigns that aim to better

51 parameterize plant hydrodynamic models.

52

1. Introduction

Tropical forests play a critical role in regulating regional and global climates (Bonan, 2008). Under ongoing and future climate change, they are subjected to substantial risks of climate extremes such as drought and heat waves (Mcdowell et al., 2018). Studies have already shown that tropical forests were experiencing elevated tree mortality rates due to mega droughts related to ENSO events. For example, the 2015–16 El Niño led to the death of an estimated 2.5 ± 0.3 billion stems in the Lower Tapajós river basin of the Amazon and the associated carbon loss had not yet been compensated by new plant growth three years after the event (Berenguer et al., 2021). Such extreme climate events are projected to increase in frequency and intensity under a warming future (Seneviratne et al., 2021). A statistical analysis based on the projection of 13 ESMs under a high greenhouse emission scenario showed that the frequency of extreme droughts as defined by rhizosphere soil moisture (occurring once every 50 years) could increase by a factor of nearly four and this increase would have a disproportionate impact on tropical forests (Xu et al., 2019). The high species diversity found in tropical forests may result in increased resilience to climate extremes, based on the demonstrated resilience of temperate forests in relationship to trait diversity (Anderegg et al., 2018). However, due to limited data to parameterize and constrain models for tropical forests, there is a large uncertainty in our predictive understanding of how tropical forests will respond to these climate extremes (Bonal et al., 2016). This tropical forest uncertainty is a key source of the global uncertainty in projections of land carbon fluxes and future climates (Arora et al., 2020).

Earth System Models (ESMs) have been developed to project future changes to the coupled climate and biosphere system. Typically, 'big leaf' approximations of vegetation with no explicit presentation of tree size and canopy structure have been used to predict the impact of vegetation on carbon and water cycles. These models do not represent the fundamental elements of vegetation dynamics including growth, mortality, competition, and their response to disturbances. In the last decade, many ESMs have incorporated vegetation demographic models (VDMs) that represent plant size, canopy structure and disturbance histories, with the goal of better representing the competitive dynamics among different size classes of trees and plant functional types in response to climate and disturbances (Fisher et al., 2018). Most of these VDMs can differentiate plants' light, water and carbon use strategies and can thus represent some part of the functional diversity of tropical forests (Massoud et al., 2019; Koven et al., 2020).

Following the 'big leaf' model, water limitation on plant gas exchange in these VDMs is generally calculated based on three factors: 1) soil water potential; 2) root distribution; and 3) water potential for stomata openness and closure, all of which differ by plant functional types (Koven et al., 2020). While these soil-moisture-dependent water limitation functions are able to capture trait diversity in leaf-level stomatal behaviors, they fail to capture plant functional diversity in many other observable plant hydraulic traits, such as xylem capacitance, water potentials for loss of xylem hydraulic conductivity, stem hydraulic safety margin, and turgor loss point (Hochberg et al., 2018). Many studies have shown that plant hydraulic traits play an important role in plant responses to droughts (Su et al., 2022; Anderegg et al., 2016), which could shape the landscape distribution of plant functional types (Kunert et al., 2021). In view of this limitation, plant hydrodynamic models have been developed with the aim of better

98   simulating forest response to droughts (Powell et al., 2018; Christoffersen et al., 2016; Xu et

99   al., 2016; Kennedy et al., 2019; Mcdowell et al., 2013). These models not only incorporate

100   hydraulic functional diversity, but also mechanistically simulate the risk of plant mortality due

101   to hydraulic functional failure, as a result of an inability to move water in the xylem due to

102   embolism in conduits (Hammond et al., 2019).

103   One key challenge for these plant hydrodynamic models is that they have many more

104   parameters than simple water limitation functions based on soil water potentials and thus

105   inherently possess more uncertainty in the model parameterization and subsequent simulations.

106   In this study, we describe the implementation of a hydrodynamic scheme within DOE-

107   sponsored functionally assembled terrestrial ecosystem simulator (FATES) (Koven et al.

108   2020), and assess this new configuration with two goals: 1) quantify the parametric sensitivity

109   of different hydraulic traits in determining plant hydrodynamics; and 2) identify key hydraulic

110   traits that are important for predicting the risk of mortality due to hydraulic failure. We expect

111   that our results will provide guidance on model parameterization for future modeling studies

112   using plant hydrodynamic models to predict tropical forest response to droughts, and future

113   field campaigns that aim to collect observational data that can be used to better parameterize

114   and benchmark plant hydrodynamic models.

115   **2. Methodology**

116   **2.1. Model description**

117   We use FATES, a VDM that is coupled within the Energy Exascale Earth System Model

118   (E3SM) (Caldwell et al., 2019). FATES represents size-structured groups of plants (cohorts)

119   and successional trajectory-based patches using the ecosystem demography approach (Fisher

120   et al., 2015; Moorcroft et al., 2001). FATES simulates growth by integrating photosynthesis

across different leaf layers for each cohort. FATES allocates this photosynthate to different tissues including leaves, fine and coarse roots, and stem, based on the allometry of different plant functional types, as well as a carbon storage pool (Fisher et al., 2015). Mortality within FATES is simulated by several mechanisms, including carbon starvation caused by depletion of the storage pool, hydraulic function failure, as well as impact mortality during disturbance, fire, logging, freezing, age-related and 'background' constant turnover (Fisher et al., 2015; Huang et al., 2020; Fisher et al., 2010; Needham et al., 2020).

2.1.1. Plant Hydrodynamics

The default (non-hydrodynamic) FATES model contains a simplistic algorithm that approximates plant hydraulic failure thresholds based on soil water potential. An important feature of the plant hydrodynamic scheme (HYDRO), which explicitly simulates water flow from the soil through leaves to the atmosphere, is that it enables direct representation of percent loss of conductance as a predictor of hydraulic failure mortality rates. FATES-HYDRO is based on the hydrodynamic model implemented in the Traits-based Forest Simulator (TFS) (Christoffersen et al., 2016) and the features most relevant to the present analysis are summarized below. The model approximates water transport in a single vertical dimension, approximating the canopy as a single leaf layer at the top of a beam, according to the Shinozaki pipe model (Shinozaki et al., 1964) in which the hydraulic path length from the trunk base to each leaf is assumed constant. Following the 'porous media' approach, the model simulates the water transport across four main organs (leaves, stem- trunk/branches, transporting roots, and absorbing roots) and different rhizosphere shells (Fig. 1). Resistors connect the different compartments.

143   The water flow is calculated based on water pressure gradients across different

144   compartments (rhizosphere, absorbing roots, transporting roots, stem, and leaf). Specifically,

145   flow between compartment i and $i + 1$ (Q_i) is given by,

146    $$Q_i = -K_i \Delta h_i, \tag{1}$$

147   where K_i is the total conductance (kg MPa^{-1} s^{-1}) at the boundary of compartments i and $i + 1$

148   and Δh_i is the total matric potential difference between the compartments,

149    $$\Delta h_i = \rho_w g (z_i - z_{i+1}) + (\psi_i - \psi_{i+1}), \tag{2}$$

150   where z_i is compartment elevation difference above (+) or below (-) the soil surface (m), ρ_w

151   is the density of water (10^3 kg m^{-3}), g is acceleration due to gravity (9.8 m s^{-2}), and ψ_i is

152   tissue or soil matric water potential (MPa). K_i is treated here as the product of a maximum

153   boundary conductance between compartments i and $i + 1$ ($K_{max,i}$), and the fractional

154   maximum hydraulic conductance of the upstream compartments (FMC_i or FMC_{i+1}), which is

155   a function of the tissue water ~~content~~potential as follows,

156    $$FMC_i = \left[1 + \left(\frac{\psi_i}{P_{50,x}} \right)^{a_x} \right]^{-1} . \tag{3}$$

157   where ψ_i is the compartmental water potential, $P_{50,x}$ is the water potential at 50% loss of

158   maximum conductivity for different plant tissues (absorbing root, transporting root, stem), a_x

159   is the corresponding vulnerability curve shape parameter, with a larger number indicating a

160   steeper reduction of conductivity in response to more negative water potentials (Choat et al.,

161   2012). The maximum percentage loss of conductivity (PLC) across different organs [i.e., PLC$_i$

162   =100 (1-FMC$_i$)] is used to measure the risk of tree mortality (M_{hf}) resulting from hydraulic

163   failure as follows,

164    $$M_{hf} = M_{hf,base} \frac{\max(0, \ PLC_{max,organ} - PLC_c)}{100 - PLC_c}, \tag{4}$$

165   where PLC_c is the critical percentage loss of conductivity with risk of mortality, $PLC_{max,organ}$

166   is the maximum percentage loss of conductivity across different organs, $M_{hf,base}$ is the

167   baseline mortality rate [fraction/year] when percentage loss of conductivity exceeds PLC_c. In

168   this version of model, we assume that xylem cavitation can fully recover as long as the trees

169   do not die.

170   The previous version of this model (TFS-Hydro) presented water in terms of relative water

171   content (RWC; g H_2O g^{-1} H_2O at saturation) in line with most empirical work on plant water

172   relations. While the underlying equations remain unchanged, here we present water in terms of

173   of volumetric water content (θ; m^3 H_2O m^{-3} plant tissue), since this what is accounted by the

174   model and is consistent with what is tracked in the soil as well. The two quantities are related

175   via the equation RWC = θ/θ_{sat}, where θ_{sat} indicates saturated volumetric water content. The

176   water potential for tissue x [ψ_x] is related to θ_x (the PV curve) following three stages of water

177   tissue drainage as follows (Tyree and Yang, 1990; Bartlett et al., 2012),

178

$$\psi_x = \begin{cases} \psi_{0,x} + m_{cap}\left(\frac{\theta_x}{\theta_{sat,x}} - 1\right) & \theta_{ft} < \theta_x \le \theta_{sat,x} \\ \psi_{sol}(\theta_x) + \psi_p(\theta_x) & \theta_{tlp,x} < \theta_x \le \theta_{ft,x} \\ \psi_{sol}(\theta_x) & \theta_{r,x} < \theta_x \le \theta_{tlp,x} \end{cases} \tag{5}$$

179   Stage one applies to stem and roots only and represents the water draw from capillary reserves

180   (embolized conduits or airspaces in wood) when wood water content is in between full turgor

181   ($\theta_{ft} = RWC_{ft}\,\theta_{sat,x}$) and saturation ($\theta_{sat,x}$) and only represents a small fraction of the total

182   PV curve. It is linear with constant slope m_{cap} = 11.3 MPa m^3 m^{-3} and RWC_{ft} = 0.958 as

183   estimated from sapwood PV curves on 28 tropical and subtropical species (Christoffersen et

184   al. 2016). RWC_{ft} is assumed to be 1.0 in leaves. Xylem water potential is assumed zero at full

185   saturation. The second stage is between full turgor ($\theta_{ft,x}$) and the turgor loss point ($\theta_{tlp,x}$),

186   when the xylem water potential is in balance with solute ($\psi_{sol}[\theta_x]$) and pressure water

187   potential ($\psi_p[\theta_x]$) of living cells. The third stage is after the turgor loss point ($\theta_{tlp,x}$), but

188   above the point of residual water content ($\theta_{r,x} = RWC_{r,x}\,\theta_{sat,x}$) where the water potential is

189   only a function of the solute water potential. $RWC_{r,x}$ is synonymous with the apoplastic

190   fraction (Bartlett et al. 2012).

191   The solute water potential is given as,

192
$$\psi_{sol}[\theta_x] = \frac{\pi_0(\theta_{sat,x}RWC_{ft} - \theta_{r,x})}{(\theta_x - \theta_{r,x})}, \tag{6}$$

193   where π_0 is the tissue osmotic potential at full turgor. The pressure potential is calculated as

194   follows,

195
$$\psi_p[\theta_x] = -|\pi_0| + \varepsilon\,\frac{(\theta_x - \theta_{sat,x}RWC_{ft})}{(\theta_{sat,x}RWC_{ft} - \theta_{r,x})}\,, \tag{7}$$

196   where ε is the bulk elastic modulus (MPa).

197   The realized conductivity of the above ground portion of the plant per unit of leaf area (

198      $K_{l,max,tree,ag}$) is calculated based on xylem hydraulic conductivity at petiole ($k_{s,max,petiole}$),

199   aboveground tree height (H, meters), and a xylem taper factor (X_{tap}) as follows,

200
$$K_{l,max,tree,ag} = \frac{k_{s,max,petiole}}{H\left(\frac{A_l}{A_s}\right)}X_{tap}, \tag{8}$$

201   where $\cancel{k_{s,max,x}}$$k_{s,max,petiole}$ is scaled from the ~~maximum~~ xylem conductivity ~~per unit sapwood~~

202   ~~area,~~measured from the branch ($k_{s,max}$) (Christoffersen et al., 2016). $\frac{A_l}{A_s}$ [i.e., la2sa in Table

203   1] is the ratio of leaf area (A_l) to sapwood area~~(A_s~~ (A_s). X_{tap} is the xylem taper factor

204   representing the ratio of aboveground xylem conductance with taper to that without, which for

205   intermediate values of conduit taper (p_taper = 1/6; see below) represents a factor increase in

206   total conductance of 23–50 for trees of heights 10–30 meters (Christoffersen et al., 2016).

207 Savage et al. (2010) highlighted how opposing selective forces will both increase hydraulic

208 conductance by the tapering of conduit radii (p_taper > 0) while at the same time protect

209 against embolism by minimizing conduit taper (no taper implies p_taper = 0). They defined

210 p_taper as the exponent on an external branching parameter (2 daughter branches per parent

211 branch in their model) that sets the degree of internal branching of xylem conduits (and thus

212 the tapering of conduit radii as well) and, using a fractal network model, derived an effective

213 exponent q that describes how aboveground conductance increases with tree size. q is a

214 monotonically increasing and saturating function of the taper exponent p (see Fig 2b of Savage

215 et al. 2010); we used this relationship to estimate q, and thus X_{tap} in eq. (8) as

216
$$X_{tap} = \left[\frac{r_{base}}{r_{petiole}}\right]^{q_{tap} - q_{notap}} , \qquad (9)$$

217 where r_{base} and $r_{petiole}$ are the trunk and petiole radii, respectively. The ratio $r_{base}/r_{petiole}$ is

218 related to tree height following the fractal tree model of Savage et al. (2010) (see equations

219 S12-S13 in Christoffersen et al. 2016).

220 Eq. (8) only gives the aboveground component of whole-plant conductance. In the

221 absence of a simple first-principles approach to estimating the belowground component, we

222 estimate the total tree maximum conductance (above- and belowground components) as

223
$$K_{max,tree,total} = R_{frac,stem} K_{max,tree,ag} , \qquad (10)$$

224 where $R_{frac,stem}$ is the fraction of total resistance that is aboveground.

225 Stomatal conductance [g_s, μmol m^{-2} s^{-1}] is simulated through a modified Ball-Berry

226 equation,

227
$$g_s = g_0 + g_1 \frac{A_n}{C_s/P_{atm}} h_s , \qquad (11)$$

228   where g_1 is the stomatal conductance slope in response to environmental condition changes,

229   g_0 is the minimum (cuticular) stomatal conductance (μmol m^{-2} s^{-1}), C_s is the leaf surface CO_2

230   partial pressure (Pa), P_{atm} is the atmospheric pressure (Pa), h_s is the leaf surface humidity,

231   and A_n is leaf net photosynthesis rate (μmol CO_2 m^{-2} s^{-1}). Stomatal conductance (i.e.,

232   both g_0 and g_1) is further modified by a plant water stress factor, β, calculated as

233
$$\beta = [1 - \left(\frac{\psi_{leaf}}{P_{50,gs}}\right)^{a_{gs}}]^{-1} , \tag{12}$$

234   where ψ_{leaf} is the leaf water potential, $P_{50,gs}$ is leaf water potential at 50% loss of maximum

235   stomatal conductance, and a_{gs} is the stomatal vulnerability shape parameter.

236   The total fine root surface area affects the amount of water a plant can take up through its

237   influence on rhizosphere conductance and is determined by both the specific root length (srl)

238   and absorbing root radius (rs2). Specifically, the model has a specified number of soil shells

239   (5 in this study) around fine root surfaces and the conductance between soil shell $k+1$ and k,

240    $K_{shell,k}$, is calculated as,

241
$$K_{shell,k} = K_s \frac{\pi \, l_{aroot,common}}{\ln(r_{k+1}/r_k)} , \tag{13}$$

242   where r_k is the mean radi of kth shell, $l_{aroot,common}$ is the total length of absorbing roots

243   calculated as a product of total fine root biomass and specific root length (srl). K_s is set to be

244   the conductance for soil (K_{soil}) when $k>1$. For $k = 1$,

245
$$K_s = \frac{1}{\frac{1}{K_{soil}} + \frac{1}{K_{root\_soil}}} , \tag{14}$$

246   where K_{root_soil} is the conductance between fine root surface and soil. An update to the TFS-

247   Hydro approach is to make this conductance direction-specific, in view that water loss rate

248   from root could be substantially lower than water uptake rate either through osmatic regulation

249   (Dichio et al., 2006) or by lacunae caused by rupture of cortical cells (North and Nobel, 1992)

250 during drought. It is determined by either the maximum uptake of water per unit of absorbing

251 root surface area ($k_{r1,max,}$ kg m^{-1} s^{-1} MPa^{-1}) when root water potential is more negative than

252 adjacent rhizosphere soil water potential, or the maximum root water loss rate per unit surface

253 area ($k_{r2,max}$, kg m^{-1} s^{-1} MPa^{-1}) when rhizosphere water potential becomes more negative than

254 root water potential, which may occur, for example, in frozen soils or in very dry soil layers

255 (Schmidhalter, 1997).

256   The plant hydrodynamic representation and numerical solver scheme within FATES-

257 HYDRO follows the 1-D solver laid out by Christoffersen et al. (2016), which is the default

258 solver in FATES-HYDRO and used in this study. The model also has an option of a 2-D solver,

259 which is slower and detailed by Fang et al. (2022) and Lambert et al. (2022). The equations

260 are solved for tissue water content at a 30 minutes time step. We made a few modifications to

261 accommodate multiple soil layers and improve the numerical stability. First, to accommodate

262 the multiple-soil layers, we sequentially solve the Richards' equation for each individual soil

263 layer, with each layer-specific solution proportional to each layer's contribution to the total

264 root-soil conductance. Second, to improve the numerical stability, we now linearly interpolate

265 the pressure/volume curve beyond the residual and saturated tissue water content to avoid the

266 rare cases of overshooting in the numerical scheme under very dry or wet conditions. See the

267 Supplementary Information [HYDRO_DESCRIPTION.pdf] for further details of the

268 implementation.

269   **2.1.2. Non-hydrodynamics processes**

270   FATES-HYDRO can be coupled to different host land models (HLMs) including the

271 E3SM land model (ELM) (Caldwell et al., 2019) or the Community Terrestrial Systems Model

272 (CTSM) (Lawrence et al., 2019). In this study, the model is coupled to ELM. In this section,

273   we layout the key non-hydrodynamic processes in the FATES or the ELM for a better

274   understanding of parameter importance in the results.

275   Canopy radiative transfer is calculated using a multi-layer scheme based on the iterative

276   Norman radiation scheme (Norman, 1979). Leaf and stem area is binned into a matrix of

277   canopy layer, leaf layer and plant functional types. Reflectance, absorption, and transmittance

278   are calculated for each leaf layer. Between canopy layers, light streams are averaged between

279   plant functional types (PFTs), such that all PFTs in understory layers receive equal radiation

280   on their top leaf layer. Fractional absorption of visible and near infra-red light is calculated

281   separately for direct and diffuse light. For the direct stream, transmitted and reflected light is

282   converted into diffuse fluxes. In FATES, the absorbed PAR is used to calculate photosynthesis

283   rates for each of the canopy layer x leaf layer x PFT bins, after which rates across layers are

284   re-aggregated into cohort level carbon fluxes. Please see the Supplementary file in Fisher et al.

285   (2015) for details.

286   The energy balance is handled by the host land model. In this study, it is based on the land

287   component of DOE's Exascale Energy Earth System Model (E3SM). The E3SM land model

288   (ELM) is based on the Community Land Model 4.5 (Oleson, 2013). Specifically, in ELM, the

289   average canopy temperature is calculated based on the energy balance of latent heat, sensible

290   heat, and absorbed radiation as determined by the radiative transfer model. The latent heat is

291   determined by the transpiration, which is determined by the vapor pressure deficit from inside

292   of leaf to the air, canopy stomatal conductance, and boundary layer conductance. FATES

293   calculated mean canopy stomatal conductance averaged across different cohorts, which is fed

294   to ELM to calculate the energy balance. The Newton-Raphson numerical scheme is used to

295   solve for the canopy temperature.

296   All aspects of soil water balance (infiltration, water transfer among soil layers, and

297   drainage) happen at the 'column' scale at 30-min time steps and are handled within the Host

298   Land Model (see Oleson et al. 2013 for a detailed description of hydrology in CLM4.5, the

299   parent model of ELM). FATES-HYDRO handles soil water operations at the patch and cohort

300   scales. It simulates root water uptake and changes in plant water potential from roots to leaves

301   based on current time step transpiration. The belowground conductance for each soil layer is

302   weighted by root biomass with an exponential vertical distribution. Sections 2 and 3 in the

303   Supplement of this manuscript provide full details on boundary conditions, sequence of

304   operations among HYDRO and the HLM, downscaling of soil moisture to rhizosphere shells,

305   and downscaling of transpiration from the patch to individual scale.

306   **2.2. Sensitivity analysis**

307   We identified 35 parameters for the FATES-HYDRO model to conduct the parametric

308   sensitivity analysis (Table 1). To estimate the parameter distributions, we started with

309   published meta-analyses (Christoffersen et al., 2016; Choat et al., 2012; Bartlett et al., 2012;

310   Bartlett et al., 2014; Bartlett et al., 2016; Klein, 2014) and supplemented them with select new

311   data from individual studies. Focal data were tissue- or individual-level hydraulic traits

312   spanning water transport and embolism resistance, tissue water storage and retention (PV curve

313   traits), hydraulic architecture (i.e., leaf area to sapwood area ratio), stomatal responses to

314   dehydration, and fine root traits (Table 1). For each dataset, we standardized taxonomic names

315   using the TNRS package in R (Boyle et al., 2013). This allowed us to join datasets together

316   based on species, averaging multiple observations per species if necessary, resulting in a

317   species-specific sparse matrix of all hydraulic traits for all databases and individual studies that

318   we compiled. This pantropical hydraulic trait dataset is included in the Supporting Information

319   [traits_master_trop.csv].

320

321   This trait dataset consisted of anywhere from 1 - 323 observations for each trait, where

322   each observation corresponds to a different species (multiple observations for the same species

323   are first averaged; see above). Before fitting distributions to these data, some traits were first

324   transformed to be positive (e.g., P50) or normalized within [0, 1] when upper and lower bounds

325   were well-defined (Table 1). Then, for each trait separately, we used the fitdistr package in R

326   to estimate best-fit parameters for uniform, beta, normal, lognormal, and gamma statistical

327   distributions in order to estimate central tendencies and spread for each trait. The distribution

328   with the largest log likelihood and best-fit parameters are given in Table 1. Each model

329   simulation consisted of a single PFT: all trees (across all cohort sizes and patches) had the

330   same traits.

331   We augmented observations with extratropical data to increase sample size for traits with

332   less than three tropics-specific observations. When trait data observations were not present, we

333   used a uniform distribution bounded on our best estimate of the theoretical range (Table 1).

334   As there is limited data on roots, we used the same distribution as that for branches if data were

335   lacking. Because our goal is to understand the model behaviors as determined by different

336   hydraulic traits, we assumed independence among traits. As we focused on the hydraulic traits

337   in this study, we used non-hydraulic trait values based on an optimal set of parameters that best

338   fit observed water and carbon fluxes in a set of FATES simulations run without hydrodynamics

339   (Koven et al., 2020).

340   We used the Fourier Amplitude Sensitivity Test (FAST) to assess the relative importance

341   of parameters in determining the variance of model outputs (Xu and Gertner, 2011a). The main

342   idea of FAST is to assign periodic signals in the sampled parameter values and use Fourier

343   transformation to identify the signals in the outputs. Sampled parameter values are based on

344   Latin hypercube sampling from the fitted statistical distributions (see previous section for more

345   details). We ran 1000 ensemble simulations of the FATES-Hydro to derive model outputs of

346   water potential and fraction of maximum conductivity. For each ensemble simulation, each

347   plant hydraulic trait was assigned with a random draw from each trait's distribution, and the

348   samples for different traits are randomly combined to sample the observed plant hydraulic trait

349   space for sensitivity analysis.

350   We used the Uncertainty Analysis and Sensitivity Analysis (UASA) tool

351   (https://sites.google.com/site/xuchongang/uasatoolbox) to estimate the parametric sensitivity

352   index, which is calculated based on the ratio of the partial variance in the model output

353   attributed to a specific parameter to the total variables in the model output. For details, please

354   refer to Xu and Gertner (2011a). We ran the model with 1000 ensemble members, in view that

355   an order of 100 times effective important number of parameters, which we estimate to be ~10,

356   is needed to achieve reasonable precision (Xu and Gertner, 2011b).

357   **2.3. Study area**

358   In this study, we used Barro Colorado Island (BCI), Panama, as our test site to evaluate

359   model behavior. We chose BCI because it has moderately strong dry and wet seasons that

360   allow us to assess the hydrodynamics under different levels of water availability. Moreover,

361   extensive field campaigns in recent years have provided comprehensive data needed for model

362   parameterization, initialization and climate drivers. Finally, we also leverage prior FATES

363   studies of non-hydraulic parameters at BCI (Koven et al., 2020).

364   BCI has an annual mean temperature of 26.3°C and an annual mean precipitation of 2656

365   mm with a strong seasonal precipitation signal. The dry season lasts from January to April,

366   with a mean precipitation of 228mm, while the wet season lasts from May-December with a

367   mean precipitation of 2428mm (Paton, 2020). In this study, we used hourly in-situ climate data

368   from 2008-2016 to drive the model. To run the model to equilibrium (in terms of soil moisture

369   content) takes 5-6 years, thus we choose February of 2016 as the target for analysis of dry

370   season hydrodynamics and August of 2016 as the target for analysis of wet season

371   hydrodynamics.

372   **2.4.   Model setup**

373   In this study, as our focus is on the plant hydrodynamics, we used the static stand structure

374   mode of FATES that turns off the processes of competition, growth and mortality, to instead

375   hold the ecosystem structure constant. This reduced-complexity configuration (Fisher and

376   Koven, 2020) thus exercises only the primarily fast-timescale-processes of photosynthesis,

377   transpiration, water transport, and plant hydrodynamics (i.e., change in hydraulic conductivity,

378   water storage, and water potentials in plant tissues). By using static stand structure mode, as in

379   Chitra-Tarak et al. (2021), we isolate hydraulic trait controls on simulated hydrodynamics and

380   avoid confounding, and potentially biased, feedbacks from resulting changes in forest

381   structure. Using static stand structure mode also means that we do not need to spin up

382   vegetation state, thus reducing the simulation time. The forest stand structure, consisting of

383   tree size and composition for each patch, is initialized based on forest inventory data collected

384   in 2015 (http://ctfs.si.edu/webatlas/datasets/bci/). As the majority of species in BCI are

385 evergreen broad leaf trees, we ran the model with one PFT with different hydraulic traits (Table

386 1) to assess their impact on the hydrodynamically relevant outputs including water potentials

387 and fraction of maximum conductivity for different plant organs including absorbing root,

388 transporting root, stem, and leaves.

389 One key benefit of utilizing a hydrodynamic model is its ability to simulate the risk of

390 hydraulic failure by considering the loss of conductivity in various plant organs. As FATES

391 model was ran on the static stand mode, we did not specifically simulate the tree mortality

392 resulting from the hydraulic failure as shown in Eq. (4). Instead, we used the maximum of loss

393 of conductance across the continuum of plant nodes [i.e., $PLC_{max,organ}$ in eq. (4)] to assess

394 the hydraulic failure risk. If $PLC_{max,organ}$ reaches critical threshold PLC_c, which is set to

395 50% (Adams et al., 2017), trees are assumed to be faced with a high risk of mortality. Using

396 the ensemble simulations, we also aim to identify the most vulnerable plant organs and the

397 critical parameters that influence the likelihood of hydraulic failure. The HDYRO model only

398 considers the stem node (Fig. 1) without explicitly simulating the branch. In this analysis, we

399 calculated the branch vulnerability by using the PLC curve of xylem and the leaf water

400 potential, which approximates the water potential at the tip of the branch. The model does not

401 explicitly consider xylary or extraxylary resistance within and outside the leaf midrib.

402 FATES simulates the carbon and water fluxes for different size classes of trees. The forest

403 has 137 cohorts with diameters ranging from 10 cm to >2 meters and height ranging from 1 to

404 38 meters (see Fig. S1 for size distributions). Because large trees experience more fluctuations

405 in environmental conditions in the canopy and higher risk of mortality due to drought (Bennett

406 et al., 2015), we focused on hydrodynamic behaviors for large trees with diameter at breast

407 height (DBH) more than 60 cm; however, for comparison, we also derived the sensitivity for

408 smaller trees with DBH less than 60 cm.

409 **3. Results**

410 Our results showed that the simulated ranges across the ensemble of leaf water potential

411 (Fig. 2) and loss of conductivity (Fig. 3) are large. For leaf water potential of large trees with

412 diameter > 60 cm, the 95% percentile ranges are from -5 MPa to -0.5 MPa and -3 MPa to -0.5

413 MPa for February (dry) and August (wet) 2016, respectively. Correspondingly, the fraction of

414 maximum stem hydraulic conductivity is much higher during August compared to February

415 (Fig. 3); however, in both months, the modeled range spans almost the full range of between 0

416 and 1. For smaller trees with diameter less than 60 cm, our results show that smaller tree

417 experienced less negative water potential (Fig. S2 and Fig. 2) and lower loss of hydraulic

418 conductivity (Fig. S3 and Fig. 3).

419 Based on the FAST sensitivity indices (i.e., the variance in model output contributed by

420 different parameters), the key parameters that control the water potentials of different plant

421 organs (leaf, stem and root) for large trees (diameter >60 cm) include the taper exponent for

422 hydraulic conductivity (*p_taper*), the water potential leading to 50% loss of stomatal

423 conductance (*p50_gs*), maximum hydraulic conductivity for the stem (*kmax_node_stem*), and

424 the fraction of total hydraulic resistance in the above ground section (*rfrac_stem*), in decreasing

425 order (Fig. 4). For the fractional loss of conductivity, the most important parameter is the water

426 potential leading to 50% loss of hydraulic conductance (P_{50}) for the corresponding organs (Fig.

427 5). Other important parameters are similar to those for simulated water potentials. Notably, the

428 organ-specific P_{50} values are more important for the dry month (February) compared to the

429 wet month (August). For the wet month of August, *p_taper* is the dominant parameter

430   controlling the pre-dawn and midday loss of hydraulic conductivity, while organ-specific P_{50}

431   parameters are the second most important. For smaller trees with diameter less than 60 cm, the

432   corresponding parametric sensitivity patterns are similar to those of larger trees (Fig. S4 and

433   Fig. S5); however, compared to larger trees, the parametric sensitivity of *p_taper* for simulated

434   leaf water potential becomes lower for smaller trees (Fig. 4 and Fig. S4).

435   In terms of the risk of hydraulic failure, out of the 1000 ensemble members, ~40% of the

436   simulations for February and ~60% of simulation for August suggest that branches are the most

437   vulnerable plant organ, based on highest loss of conductivity across the continuum from root

438   to branch (Fig. 6). For the dry month of February, roots are at greater risk in comparison to the

439   wet season. If we consider the loss of conductivity more than 50% for February 2016 as a

440   threshold for a high risk of mortality (Adams et al., 2017), then 53% of ensemble simulations

441   reach this threshold. The key parameters affecting the risk of mortality, as measured by

442   percentage difference in parameter values for ensemble members reaching 50% loss of

443   conductivity or not, include the water potential leading to 50% loss of conductance for stomata

444   (*p50_gs*), stem (*p50_node_stem*), and transporting roots (*p50_node_troot*), maximum

445   hydraulic conductivity of stem (*kmax_node_stem*), and the taper exponent (*p_taper*) (Fig. 7).

446   Ensemble members with high risk of mortality generally have a higher *p_taper* and

447   *kmax_node_stem*, less negative *p50_gs*, and less negative p50 for stem and transporting roots

448   (Fig. 8).

449   **4. Discussion**

450   Our analysis showed the importance of key plant hydraulic traits in simulating plant water

451   potential and risk of hydraulic failure. This analysis identifies these parameters as potential

452   targets of either model calibration or targeted measurement campaigns to achieve realistic

simulations. In our sensitivity analysis, the most influential parameter for both water potential and loss of conductivity is the tapering of the radius of conduit with increasing plant height (p_taper). As p_taper increases, the conduit radius increases from the top of the tree to its base. According to Hagen-Poiseuille's equation, this increases the theoretical maximum total conductance. Low values of p_taper thus limit the adverse effects of tree height by increasing k_max along the whole continuum and reducing the soil-to-leaf water potential needed to maintain transpiration. Our inference is that p_taper represents an overarching property of plant architecture that influences the relative effect of each of the other traits related to hydraulic safety and efficiency (Olson et al., 2021). The xylem architecture as determined by p_taper parameter could change in response to age and development stages (Rodriguez-Zaccaro et al., 2019), which is not considered in this study. Future studies evaluating the importance of this change to hydraulic functions could be useful to guide size-dependent growth and mortality. Another dimension of the hydraulic architecture with a critical role in determining both water potential and loss of conductivity, though to a much lesser degree, was the fraction of total tree resistance that is belowground (i.e., of the entire transporting and absorbing root system; 1- $rfrac\_stem$). Generally, a plant will match the growth of its trunk and crown to maintain a degree of equilibrium in aboveground resistance as the distance water needs to travel increases (Yang and Tyree, 1993). In this study, due to the lack of data on the belowground resistance, we assigned a quite large range for this trait, which could be impacted by many factors such as belowground root biomass, root network architecture, and interactions between roots, fungi and bacteria (Poudel et al., 2021; Bhagat et al., 2021).

The second most sensitive parameter in determining loss of conductance was the leaf water potential at 50% loss of stomatal conductance ($p50\_gs$). This parameter controls the water loss

476   rate from leaves, with a less negative value providing protection from hydraulic failure during

477   water-limited periods. The *p50_gs* trait has been shown to play a key role in tree survival

478   during severe droughts (Breshears et al., 2009; Rowland et al., 2015). The ability to withstand

479   lower leaf water potentials is also a key indicator of sapling and seedling survival during

480   drought and determines species distribution across a moisture gradient (Kursar et al., 2009).

481   There may be a trade-off between drought tolerance (with a lower *p50_gs*) and drought

482   avoidance (a less negative *p50_gs* but with a high capacitance; the amount of water released

483   from reserves as leaf water potential declines), a crucial aspect in determining species drought

484   resistance (Pineda-Garcia et al., 2013). Additionally, loss of conductivity was sensitive to the

485   water potential at 50% loss of max conductivity within the stem (*p50_stem*) as it can largely

486   affect the whole plant conductance and thus the water supply to the leaves. *p50_stem*

487   negatively correlates with wood density and may be a marker of the trade-off between

488   hydraulic efficiency and safety within the stem (Chen et al., 2009; Manzoni et al., 2013);

489   however, other studies have shown that this trade-off is weak (Gleason et al., 2016). Liang et

490   al (2019) showed that the strength of this trade-off could be dependent on specie's drought

491   strategies.

492   Leaf water potential and loss of conductance were both sensitive to the maximum xylem

493   conductivity in the stem (*kmax_node_stem*). Higher maximum conductivity represents greater

494   xylem efficiency, which in the absence of drought or light limitations would result in greater

495   potential photosynthesis and less negative water potentials (Gleason et al., 2016). However,

496   xylem with higher *kmax_node_stem* could be more vulnerable to embolism as water potential

497   declines (Sperry and Love, 2015). In tropical rainforests, species with higher conductivity per

498   unit leaf area generally are less desiccation-tolerant, and thus exhibit higher mortality rates

499   (Kursar et al., 2009). Low *kmax_node_stem* along with high leaf-to-sapwood area ratio (*la2sa*)

500   also represents a vulnerability to reduced conductance which increases with height

501   (Christoffersen et al., 2016).

502   Traits with lower order of impacts on water potential modulate the amount of stored water

503   available during drought. The bulk modulus of elasticity in the root (*epsil_node_aroot*)

504   together with root saturated water content determines the amount of water available from

505   cellular storage between complete hydration and loss of turgor (Powell et al., 2017). This

506   represents the ability of the roots to continually supply water to the rest of the plant as drought

507   occurs. It also represents an investment in cellular structure, which may be an additional

508   indicator of adaptations with non-hydraulic origin. The residual water content in the stem

509   (*resid_node_stem*) determines the minimum amount of water xylem will hold and thus impact

510   the amount of water storage plant can use during drought as well (Bartlett et al. 2012). In this

511   study, we made the assumption that the traits are independent of each other, in order to

512   understand the hydrodynamic behaviors of FATES-HYDRO for different hydraulic traits

513   based on a single PFT. Understanding the trade-offs between these traits is crucial for

514   determining the competition among different PFTs. Future studies would greatly benefit from

515   assessing the significance of these trade-offs to predict vegetation dynamics under future

516   climate change.

517   In contrast to the majority of hydraulic traits in the model, conduit taper, the fraction of

518   total resistance belowground, and the leaf to sapwood area ratio are whole-plant hydraulic

519   traits. Our analysis highlights the importance of whole-plant hydraulic traits such as conduit

520   taper relative to tissue-level hydraulic traits for a range of plant hydraulic functions, including

521   whole-plant conductance and hydraulic failure risks. An important area for future work is to

better constrain and understand the consequences of intra- and interspecific variation in these whole-plant hydraulic traits in tropical forests. Our choice of the range of variation in the conduit taper exponent came from a study on temperate species, and was broad, encompassing the entire range of observed values in that study (Savage et al. 2010). Further, we estimated the effects of variation in the taper exponent on whole-plant conductance conditional on trees following a simple set of optimality assumptions (space-filling, area-conserving, and self-similar branching network structure). However, in practice, such assumptions are often not met (Smith et al., 2014). Therefore, it is possible that the model sensitivity to xylem taper in terms of whole-plant hydraulic function are overestimated. Nevertheless, our study highlights the importance of better constraining this parameter as well as further experimentation with alternate model structures to better account for non-optimal trees in tropical forests.

The sensitivity of vegetation to drought stress and hydraulic-failure-induced mortality is of paramount importance for understanding how ecosystems may respond to shifting temperature and rainfall patterns under a changing climate (Mcdowell et al., 2022). We recognize that parametric sensitivity could be different for different sites depending on climate driver, soil moisture and vegetation types. However, we expect the main parameter of importance could be useful to guide model calibration to select the candidate parameters for different sites. As understanding of plant hydrodynamics increases, linking model predictions to observable plant traits has emerged as a promising means of constraining predictions of ecosystem resilience. Such traits are challenging and costly to measure in the field and thus resources must be directed carefully when planning measurement campaigns. The identified parameters in this study could provide guidance on the limited measurement we could target in the field.

5. Acknowledgment

545 This research was supported as part of the Next Generation Ecosystem Experiments-

546 Tropics, funded by the U.S. Department of Energy, Office of Science, Office of Biological and

547 Environmental Research. RF acknowledges funding by the European Union's Horizon 2020

548 (H2020) research and innovation program under Grant Agreement No. 101003536 (ESM2025

549 – Earth System Models for the Future) and 821003 (4C, Climate-Carbon Interactions in the

550 Coming Century).

551 **6. CODE and Data Availability**

552 The FATES-HYDRO code is available from https://doi.org/10.5281/zenodo.7686333. The

553 traits data are in the supplementary file [traits_master_trop.csv].

554 **7. Supplement Information**

555 Three supplementary file are included. The HYDRO_DESCRIPTION.pdf provide the

556 summary of the hydrodynamic implementation that is different from Christoffersen et al.

557 (2016). The traits_master_trop.csv file include all the hydraulic traits we assembled for the

558 tropical region. The supplementary_figure.pdf provides additional figures for the main text.

559 **8. Author contribution**

560 CX and BC designed the sensitivity analysis experiments. BC collected the data and fitted

561 the trait distributions. CX conducted the analysis and drafted the manuscript. BC, CX, RF, RN

562 and CK designed the implementation of HYDRO codes. BC implemented the majority of

563 HYDRO codes with code improvement made by CX and RN. ZR conducted the ensemble

564 model simulations. MS provided the leaf cuticular conductance data. NM, CK and LK

565 provided guidance on the sensitivity analysis, code development and trait data synthesis. All

566 authors contributed to manuscript writing by providing edits and suggestions.

567 **9. Competing interests**

568   The contact author has declared that none of the authors has any competing interests.

569

570

Figures

572

573
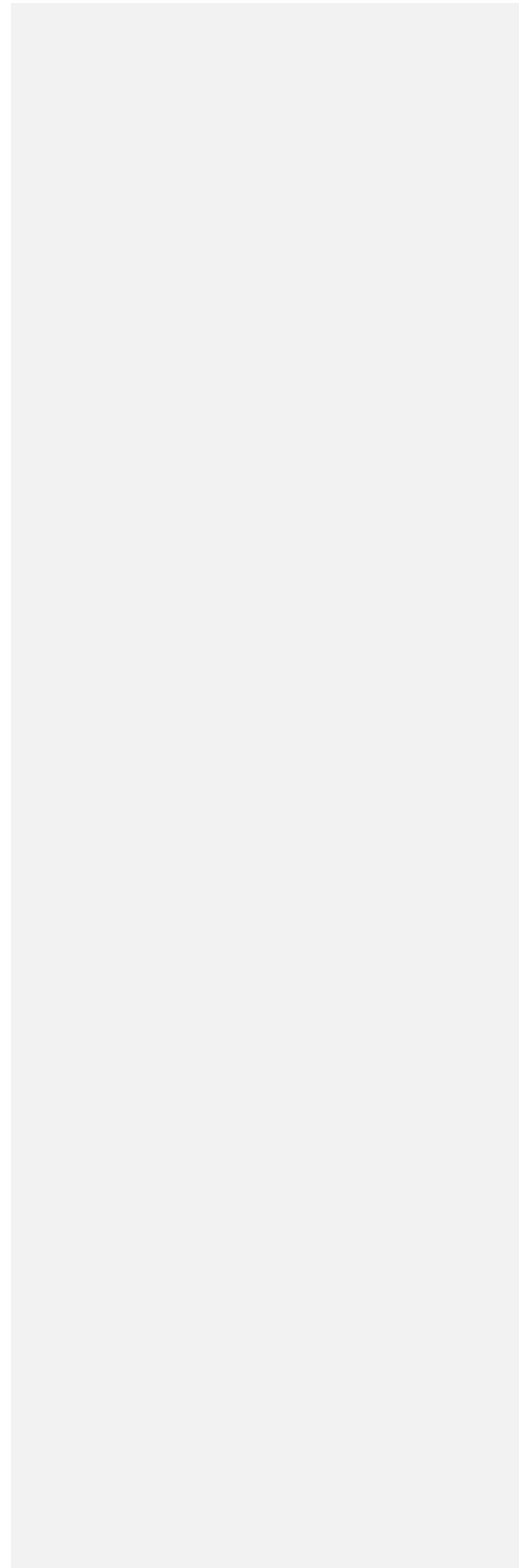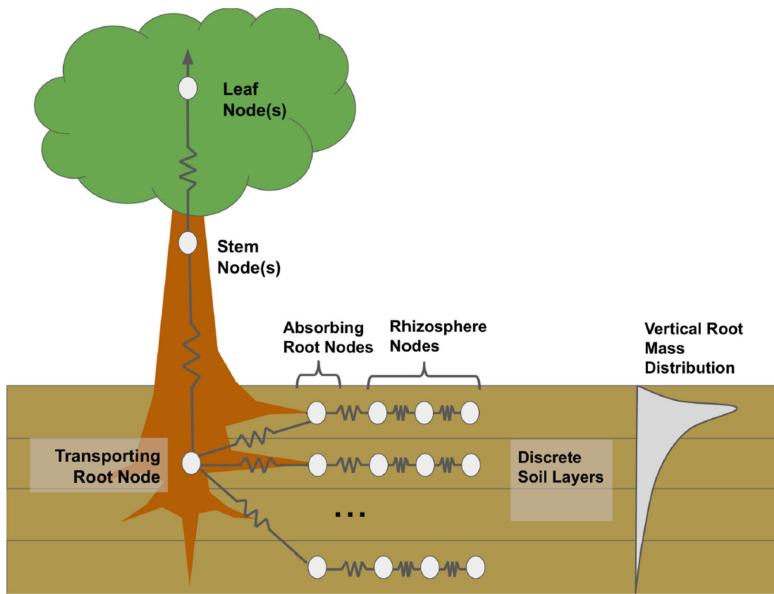
Figure 1: Diagram of FATES-HYDO with simulation of rhizosphere shell, absorbing roots, transporting roots, stem and

leaves. The model is solved for different soil layers with different root distributions.

576

577

578

579

580

581
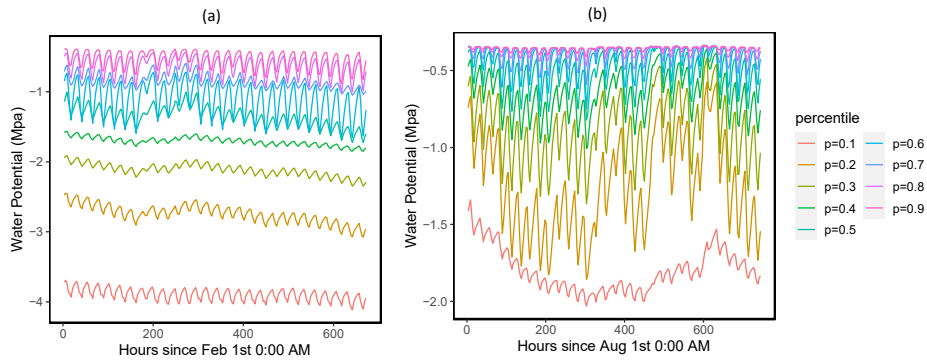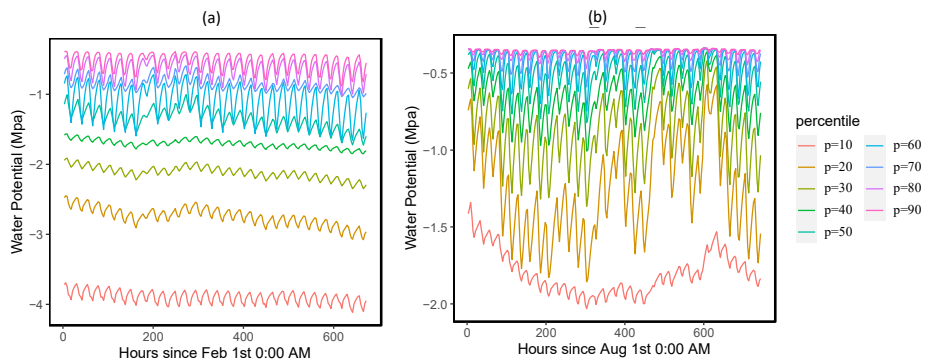
Figure 2: Simulated ranges of leaf water potential for February (a) and August (a), 2016 for trees with DBH > 60cm. The

percentiles are calculated based on the monthly mean values of leaf water potentials for the 1000 ensemble simulations.

584

585

586

587
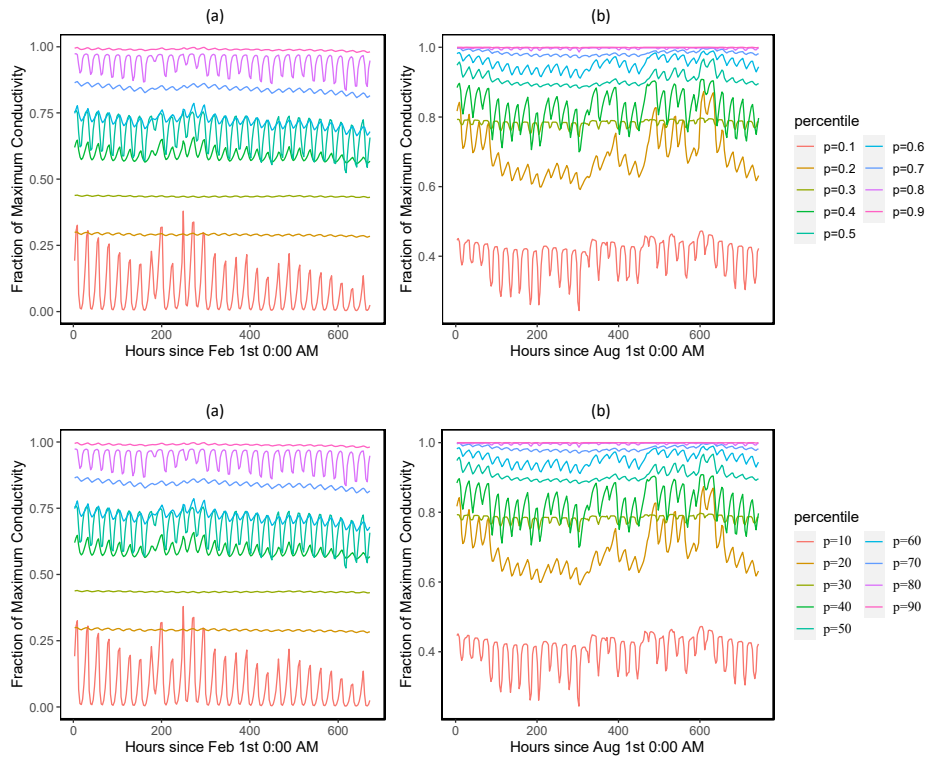
588 **Figure 3: Simulated ranges of fraction of maximum hydraulic conductivity of stem for February (a) and August (a), 2016**

589 **for trees with DBH > 60cm**. The percentiles are calculated based on the monthly mean values of leaf water potentials for the

590 1000 ensemble simulations.

591

592
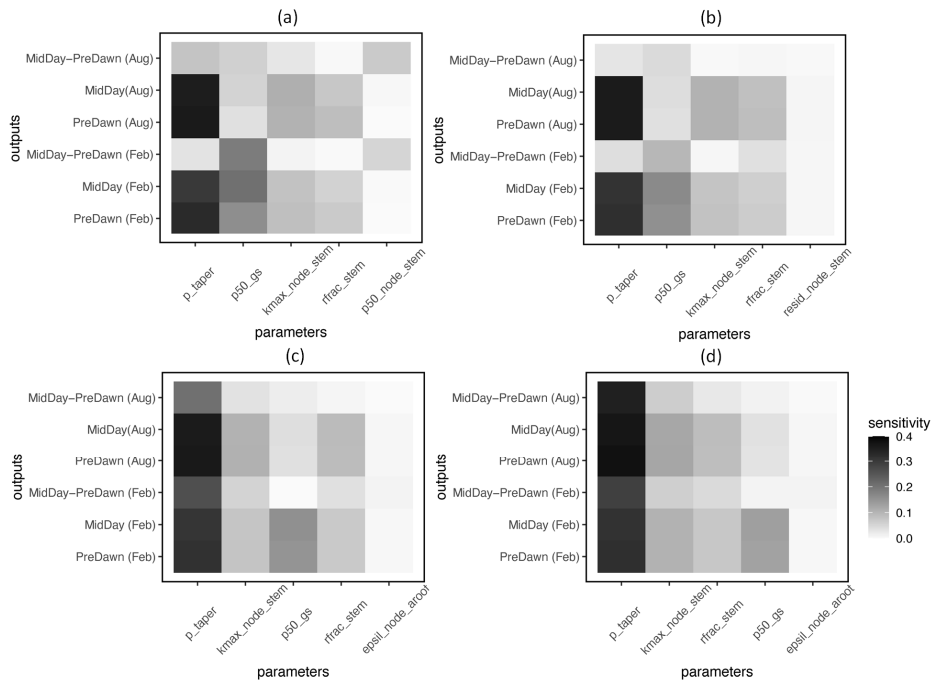
593
594 **Figure 4: Key parameters that control simulated water potentials for leaf (a), stem (b), transporting root (c) and**

595 **absorbing root (d), for trees with DBH > 60cm.** The sensitivity value refers to the proportion of total model output variance

596 contributed by a specific parameter (0-1). See Table 1 for the explanation of the parameters.

597
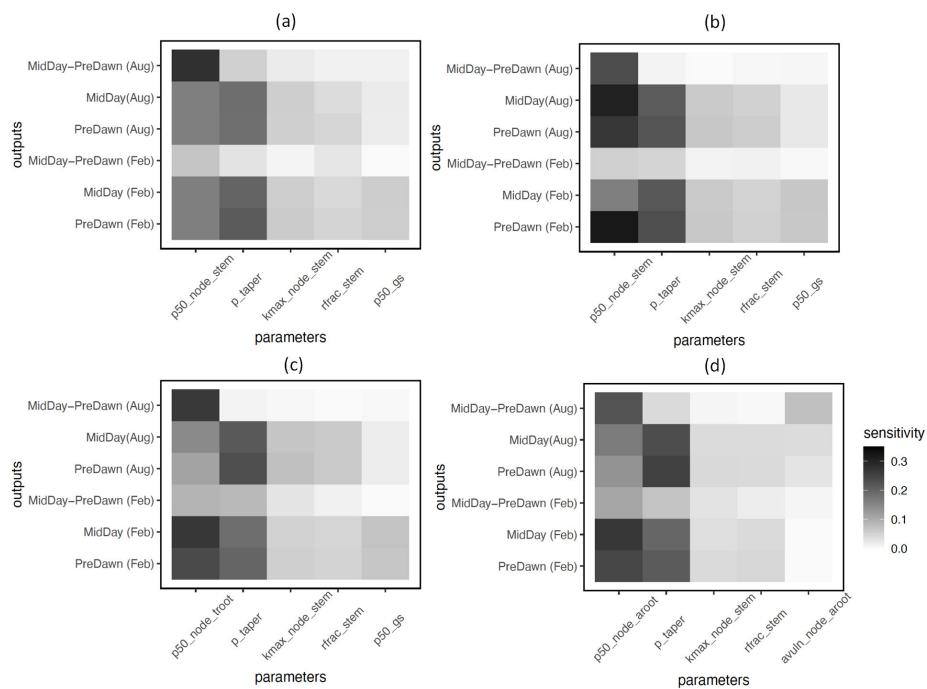
598

599

600 **Figure 5: Key parameters that control simulated loss of conductivity for branch (a), stem (b), transporting root (c) and**

601 **absorbing root (d), for trees with DBH > 60cm.** The sensitivity value refers to the proportion of total model output variance

602 contributed by a specific parameter. See Table 1 for the explanation of the parameters. See Table 1 for the description of

603 parameters.

604

605
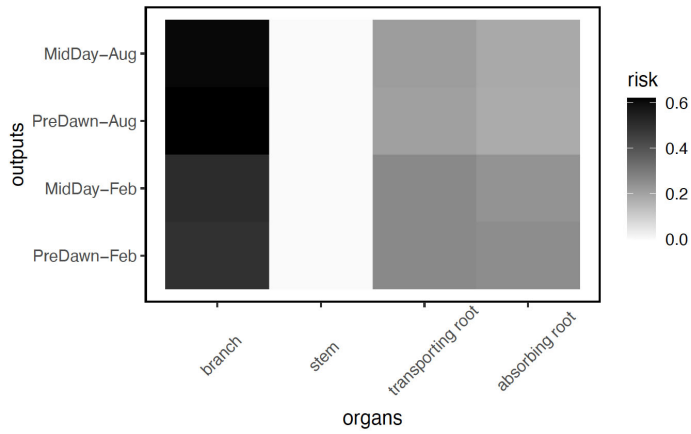
Figure 6: Risk on the continuum for hydraulic failure as measured by percentage of total number of simulations with

highest loss of conductivity for a specific organ (branch, stem, transporting root and absorbing root), for trees with DBH

> 60cm. As the model does not specifically simulate the branch, we calculated the risk of loss of conductivity based on the leaf

water potential and hydraulic vulnerability curve from xylem.

610

611

612

613

614
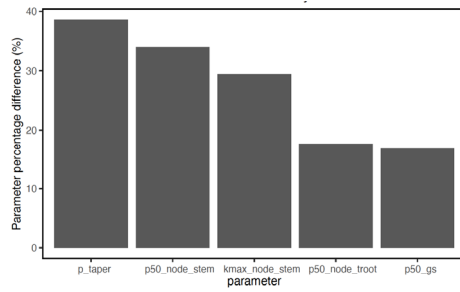
Figure 7: Mean trait percentage difference for model ensemble simulations with loss of hydraulic conductivity larger than 50% and ensemble simulations with loss of hydraulic conductivity less than 50%, for trees with DBH > 60cm. See Table 1 for the description of parameters.

618

619

620
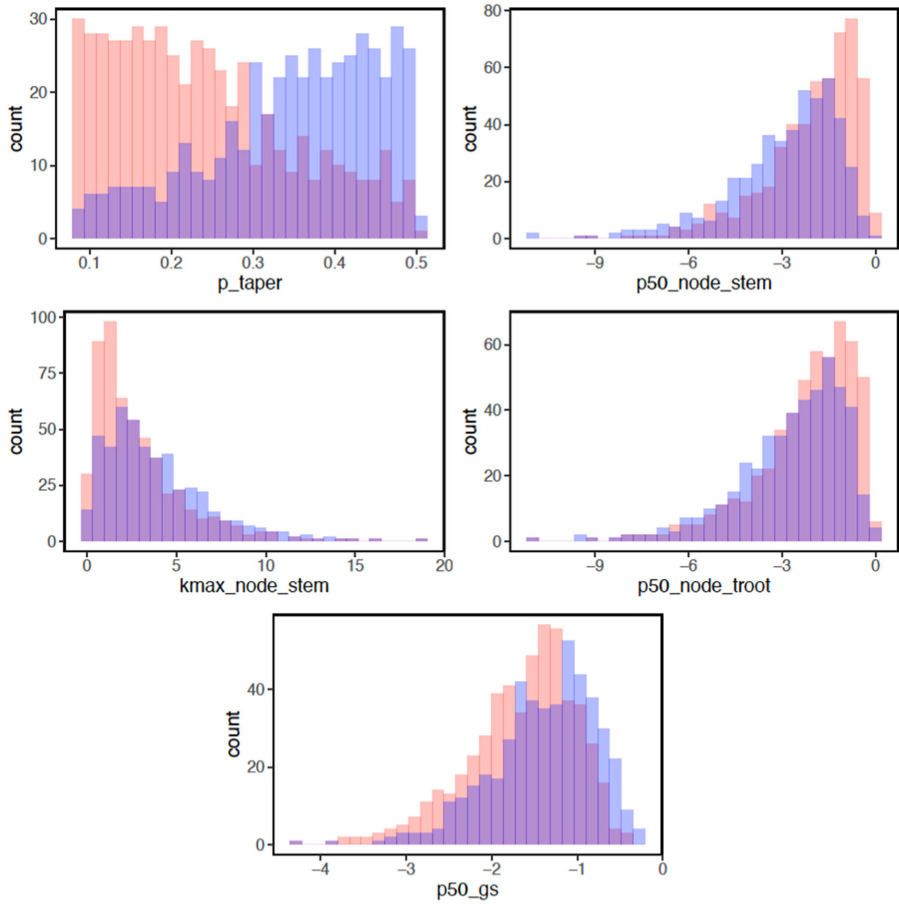
Figure 8: Parameter difference for ensemble members with risk of mortality, for trees with DBH > 60cm. Blue bars
indicate parameter values with lower mortality risk (<50% loss of hydraulic conductivity). Red bars indicate parameter values
with higher mortality risk (>= 50% loss of hydraulic conductivity) and purple bars indicate parameter values stacked from
transparent red/blue bars. See Table 1 for the description of parameters.

625

626

627
628 Table 1 Hydraulic parameters considered in the sensitivity analysis

Parameter (equation number)[1]	~~Symbol~~Symbol[2]	Units	~~Distribution[1]~~Distribution[3]	Sources & Notes
Pressure-Volume (PV) curve (water content – water potential relationship)				
saturated water content (thetas_node_leaf, thetas_node_stem, thetas_node_troot, thetas_node_aroot) (Eq. 5)	$\theta_{sat,x}$	cm^3 cm^{-3}	Leaf: Beta (9.69, 6.20) Stem: Beta (12.67, 7.4626) TRoot and ~~AROOT~~ARoot: Beta (22.98, 5.29)	Christoffersen et al. (2016) Iversen et al. (2017) Wright et al. (2010) Roderick et al. (1999) Sack et al. (2003) Binks et al. (2016)
turgor loss point (tlp_node_leaf, tlp_node_stem, tlp_node_troot, tlp_node_aroot) (Eq. 5)	~~π_{tlp}~~$\pi_{tlp,x}$	MPa	$\pi_{tlp} = (\pi_0\,\varepsilon)\,/(\pi_0 + \varepsilon)$	Bartlett et al. (2012) Christoffersen et al. (2016)
osmotic potential at full turgor (pinot_node_leaf, pinot_node_stem, pinot_node_troot, pinot_node_aroot) (Eq. 6)	~~π_0~~$\pi_{0,x}$	MPa	Leaf: G [9.8,6.26], Stem, TRoot, ARoot: LN [0.32,0.39]	Bartlett et al. (2012, 2014, 2016) ~~and~~ Christoffersen et al. (2016)
bulk elastic modulus (epsil_node_leaf, epsil_node_stem, epsil_node_troot, epsil_node_aroot) (Eq. 7)	~~ε~~ε_x	MPa	Leaf: G (4.07, 4.12) Stem, TRoot and ARoot: G [3.57, 3.84]	Bartlett et al. (2012, 2014~~),~~ ~~and)~~ Christoffersen et al. (2016)
residual water fraction (resid_node_leaf, resid_node_stem, resid_node_troot, resid_node_aroot) (Eq. 5)	~~RWC_r~~RWC	unitless	Leaf: B [2.14,4.10] Stem, TRoot and ARoot: B [2.71, 4.53]	Bartlett et al. (2012, 2014~~),)~~ Christoffersen et al. (2016)
Vulnerability Curve (water potential – hydraulic conductivity relationship)				
water potential at 50% loss of max conductivity (p50_node_stem, p50_node_troot, p50_node_aroot) (Eq. 3)	$P_{50,x}$	MPa	Stem, TRoot and ARoot: G [2.07, 1.18]	Choat et al. (2012)
vulnerability curve shape parameter (avuln_node_stem, avuln_troot, avuln_node_aroot) (Eq. 3)	a_x	unitless	Stem, TRoot and ARoot: LN [0.82, 0.66]	Choat et al. (2012)

xylem conductivity per unit sapwood area (kmax_node_stem) (Eq. ~~7~~8)	$k_{s,max}k_{s,m}$	kg m^{-1} s^{-1} MPa^{-1}	G [1.41, 2.37]	Choat et al. (2012)
Leaf hydraulics				
leaf water potential at 50% loss of max gs (p50_gs) (Eq. 12)	$P_{50,gs}$	MPa	G [5.73, 0.27]	Klein (2014)
stomatal vulnerability shape parameter(avuln_gs) (Eq. 12)	a_{gs}	unitless	a_{gs}= -2.406 P50,gs (-P50,gs) $^{-1.25}$	Christoffersen et al. (2016)
Leaf cuticular conductivity (k0_leaf) (Eq. 11)	g_0	umol m^{-2}s^{-1}	LN [1.04, 0.84]	~~This study (M. Slot, unpublished data)~~Slot et al. (2021)
Plant Hydraulic Architecture				
Xylem taper exponent for sapwood (p_taper) (Eq. 9)	p	(-)	U (0.08, 0.5)	Savage et al. (2010)
Leaf area to sapwood area ratio (la2sa) (Eq. ~~7~~8)	$\frac{A_l}{A_s}$	(-)	LN (-0.48, 0.77)	Choat et al. (2012)
Root hydraulic Traits				
specific root length (*srl*) (Eq. 13)	srl	m g^{-1}	G [1.70, 35.31]	Iversen et al. (2017)
absorbing root radius (*rs2*) (Eq. 13)	r	mm	LN [-1.91, 0.79]	Iversen et al. (2017)
fraction of total tree resistance that is aboveground (*rfrac_stem*) (Eq. 10)	$R_{frac,stem}$	Unitless	U [0.1,0.7]	This study; empirical
root-soil interface conductivity per unit surface area (K_{r1}) (Eq. ~~13~~14)	$k_{r1,max}$	kg m^{-1} s^{-1} MPa^{-1}	G [1.41, 2.37]	This study; empirically set the same as xylem conduct...
maximum root water loss rate (K_{r2}) (Eq. 14)	$k_{r2,max}$	kg m^{-1} s^{-1} MPa^{-1}	LN [-6.80, 0.92]	Wolfe (2020); Empiri... as 1/1000 bark water loss rate

629 ~~Note: 1~~**Note:** 1: Several hydraulic parameters are used for different nodes of the plant including leaf,

630 stem, transporting root (troot), and absorbing root (aroot). For better reference in the text, we provided a

631 list of these parameters for specific nodes in the parenthesis; 2: Subscript *x* represents different tissue

632 nodes in the model; 3:B-Beta distribution; U- Uniform distribution [lower limit, upper limit]; N-

633   Gaussian distribution (mean, standard deviation); LN-Log Normal Distribution [mean, standard

634   deviation]; G-Gamma distribution (lambda, scale); TRoot-Transporting root; ARoot-Absorbing root.

635
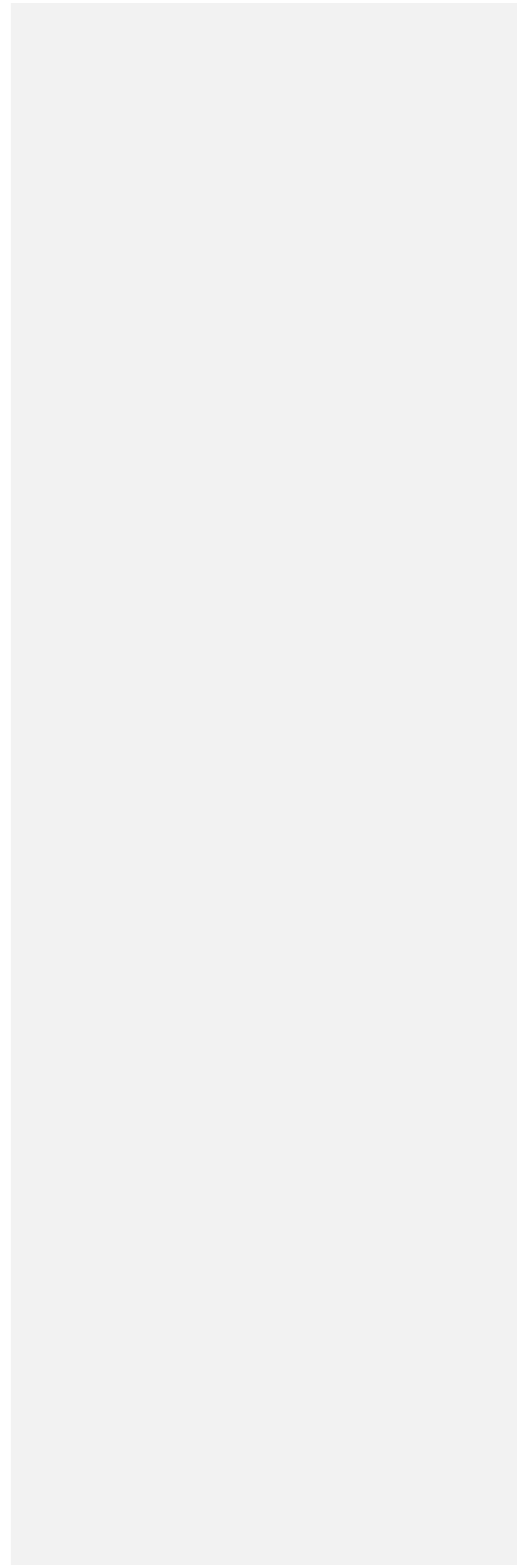
636 **Reference**

637 Adams, H. D., Zeppel, M. J. B., Anderegg, W. R. L., Hartmann, H., Landhausser, S. M., Tissue,
638 D. T., Huxman, T. E., Hudson, P. J., Franz, T. E., Allen, C. D., Anderegg, L. D. L., Barron-
639 Gafford, G. A., Beerling, D. J., Breshears, D. D., Brodribb, T. J., Bugmann, H., Cobb, R. C.,
640 Collins, A. D., Dickman, L. T., Duan, H. L., Ewers, B. E., Galiano, L., Galvez, D. A., Garcia-
641 Forner, N., Gaylord, M. L., Germino, M. J., Gessler, A., Hacke, U. G., Hakamada, R., Hector,
642 A., Jenkins, M. W., Kane, J. M., Kolb, T. E., Law, D. J., Lewis, J. D., Limousin, J. M., Love, D.
643 M., Macalady, A. K., Martinez-Vilalta, J., Mencuccini, M., Mitchell, P. J., Muss, J. D., O'Brien,
644 M. J., O'Grady, A. P., Pangle, R. E., Pinkard, E. A., Piper, F. I., Plaut, J. A., Pockman, W. T.,
645 Quirk, J., Reinhardt, K., Ripullone, F., Ryan, M. G., Sala, A., Sevanto, S., Sperry, J. S., Vargas,
646 R., Vennetier, M., Way, D. A., Xu, C. G., Yepez, E. A., and McDowell, N. G.: A multi-species
647 synthesis of physiological mechanisms in drought-induced tree mortality, Nat Ecol Evol, 1,
648 1285-1291, 10.1038/s41559-017-0248-x, 2017.
649 Anderegg, W. R. L., Klein, T., Bartlett, M., Sack, L., Pellegrini, A. F. A., Choat, B., and Jansen,
650 S.: Meta-analysis reveals that hydraulic traits explain cross-species patterns of drought-induced
651 tree mortality across the globe, P Natl Acad Sci USA, 113, 5024-5029,
652 10.1073/pnas.1525678113, 2016.
653 Anderegg, W. R. L., Konings, A. G., Trugman, A. T., Yu, K. L., Bowling, D. R., Gabbitas, R.,
654 Karp, D. S., Pacala, S., Sperry, J. S., Sulman, B. N., and Zenes, N.: Hydraulic diversity of forests
655 regulates ecosystem resilience during drought, Nature, 561, 538–541, 10.1038/s41586-018-0539-
656 7, 2018.
657 Arora, V. K., Katavouta, A., Williams, R. G., Jones, C. D., Brovkin, V., Friedlingstein, P.,
658 Schwinger, J., Bopp, L., Boucher, O., Cadule, P., Chamberlain, M. A., Christian, J. R., Delire,
659 C., Fisher, R. A., Hajima, T., Ilyina, T., Joetzjer, E., Kawamiya, M., Koven, C. D., Krasting, J.
660 P., Law, R. M., Lawrence, D. M., Lenton, A., Lindsay, K., Pongratz, J., Raddatz, T., Seferian,
661 R., Tachiiri, K., Tjiputra, J. F., Wiltshire, A., Wu, T. W., and Ziehn, T.: Carbon-concentration
662 and carbon-climate feedbacks in CMIP6 models and their comparison to CMIP5 models,
663 Biogeosciences, 17, 4173-4222, 10.5194/bg-17-4173-2020, 2020.
664 Bartlett, M. K., Scoffoni, C., and Sack, L.: The determinants of leaf turgor loss point and
665 prediction of drought tolerance of species and biomes: a global meta-analysis, Ecol Lett, 15, 393-
666 405, 10.1111/j.1461-0248.2012.01751.x, 2012.
667 Bartlett, M. K., Klein, T., Jansen, S., Choat, B., and Sack, L.: The correlations and sequence of
668 plant stomatal, hydraulic, and wilting responses to drought, P Natl Acad Sci USA, 113, 13098-
669 13103, 10.1073/pnas.1604088113, 2016.
670 Bartlett, M. K., Zhang, Y., Kreidler, N., Sun, S. W., Ardy, R., Cao, K. F., and Sack, L.: Global
671 analysis of plasticity in turgor loss point, a key drought tolerance trait, Ecol Lett, 17, 1580-1590,
672 10.1111/ele.12374, 2014.
673 Bennett, A. C., McDowell, N. G., Allen, C. D., and Anderson-Teixeira, K. J.: Larger trees suffer
674 most during drought in forests worldwide, Nat Plants, 1, Artn 15139
675 10.1038/Nplants.2015.139, 2015.
676 Berenguer, E., Lennox, G. D., Ferreira, J., Malhi, Y., Aragao, L. E. O. C., Barreto, J. R.,
677 Espirito-Santo, F. D., Figueiredo, A. E. S., Franca, F., Gardner, T. A., Joly, C. A., Palmeira, A.
678 F., Quesada, C. A., Rossi, L. C., de Seixas, M. M. M., Smith, C. C., Withey, K., and Barlow, J.:
679 Tracking the impacts of El Nino drought and fire in human-modified Amazonian forests, P Natl
680 Acad Sci USA, 118, ARTN e2019377118: 10.1073/pnas.2019377118, 2021.

681 Bhagat, N., Raghav, M., Dubey, S., and Bedi, N.: Bacterial Exopolysaccharides: Insight into
682 Their Role in Plant Abiotic Stress Tolerance, J Microbiol Biotechn, 31, 1045-1059,
683 10.4014/jmb.2105.05009, 2021.
684 Binks, O., Meir, P., Rowland, L., da Costa, A. C. L., Vasconcelos, S. S., de Oliveira, A. A. R.,
685 Ferreira, L., Christoffersen, B., Nardini, A., and Mencuccini, M.: Plasticity in leaf-level water
686 relations of tropical rainforest trees in response to experimental drought, New Phytol, 211, 477-
687 488, 10.1111/nph.13927, 2016.
688 Bonal, D., Burban, B., Stahl, C., Wagner, F., and Herault, B.: The response of tropical rainforests
689 to drought-lessons from recent research and future prospects, Ann Forest Sci, 73, 27-44,
690 10.1007/s13595-015-0522-5, 2016.
691 Bonan, G. B.: Forests and climate change: Forcings, feedbacks, and the climate benefits of
692 forests, Science, 320, 1444-1449, 10.1126/science.1155121, 2008.
693 Boyle, B., Hopkins, N., Lu, Z., Raygoza Garay, J. A., Mozzherin, D., Rees, T., Matasci, N.,
694 Narro, M. L., Piel, W. H., and Mckay, S. J.: The taxonomic name resolution service: an online
695 tool for automated standardization of plant names, BMC bioinformatics, 14, 1-15, 2013.
696 Breshears, D. D., Myers, O. B., Meyer, C. W., Barnes, F. J., Zou, C. B., Allen, C. D., McDowell,
697 N. G., and Pockman, W. T.: Tree die-off in response to global change-type drought: mortality
698 insights from a decade of plant water potential measurements, Front Ecol Environ, 7, 185-189,
699 10.1890/080016, 2009.
700 Caldwell, P. M., Mametjanov, A., Tang, Q., Van Roekel, L. P., Golaz, J. C., Lin, W. Y., Bader,
701 D. C., Keen, N. D., Feng, Y., Jacob, R., Maltrud, M. E., Roberts, A. F., Taylor, M. A.,
702 Veneziani, M., Wang, H. L., Wolfe, J. D., Balaguru, K., Cameron-Smith, P., Dong, L., Klein, S.
703 A., Leung, L. R., Li, H. Y., Li, Q., Liu, X. H., Neale, R. B., Pinheiro, M., Qian, Y., Ullrich, P.
704 A., Xie, S. C., Yang, Y., Zhang, Y. Y., Zhang, K., and Zhou, T.: The DOE E3SM Coupled
705 Model Version 1: Description and Results at High Resolution, J Adv Model Earth Sy, 11, 4095-
706 4146, 10.1029/2019ms001870, 2019.
707 Chen, J. W., Zhang, Q., Li, X. S., and Cao, K. F.: Independence of stem and leaf hydraulic traits
708 in six Euphorbiaceae tree species with contrasting leaf phenology, Planta, 230, 459-468,
709 10.1007/s00425-009-0959-6, 2009.
710 Chitra-Tarak, R., Xu, C. G., Aguilar, S., Anderson-Teixeira, K. J., Chambers, J., Detto, M.,
711 Faybishenko, B., Fisher, R. A., Knox, R. G., Koven, C. D., Kueppers, L. M., Kunert, N., Kupers,
712 S. J., McDowell, N. G., Newman, B. D., Paton, S. R., Perez, R., Ruiz, L., Sack, L., Warren, J.
713 M., Wolfe, B. T., Wright, C., Wright, S. J., Zailaa, J., and McMahon, S. M.: Hydraulically-
714 vulnerable trees survive on deep-water access during droughts in a tropical forest, New Phytol,
715 231, 1798-1813, 10.1111/nph.17464, 2021.
716 Choat, B., Jansen, S., Brodribb, T. J., Cochard, H., Delzon, S., Bhaskar, R., Bucci, S. J., Feild, T.
717 S., Gleason, S. M., Hacke, U. G., Jacobsen, A. L., Lens, F., Maherali, H., Martinez-Vilalta, J.,
718 Mayr, S., Mencuccini, M., Mitchell, P. J., Nardini, A., Pittermann, J., Pratt, R. B., Sperry, J. S.,
719 Westoby, M., Wright, I. J., and Zanne, A. E.: Global convergence in the vulnerability of forests
720 to drought, Nature, 491, 752-+, 10.1038/nature11688, 2012.
721 Christoffersen, B. O., Gloor, M., Fauset, S., Fyllas, N. M., Galbraith, D. R., Baker, T. R., Kruijt,
722 B., Rowland, L., Fisher, R. A., Binks, O. J., Sevanto, S., Xu, C. G., Jansen, S., Choat, B.,
723 Mencuccini, M., McDowell, N. G., and Meir, P.: Linking hydraulic traits to tropical forest
724 function in a size-structured and trait-driven model (TFS v.1-Hydro), Geosci Model Dev, 9,
725 4227-4255, 10.5194/gmd-9-4227-2016, 2016.

726 Dichio, B., Xiloyannis, C., Sofo, A., and Montanaro, G.: Osmotic regulation in leaves and roots
727 of olive trees during a water deficit and rewatering, Tree Physiol, 26, 179-185, DOI
728 10.1093/treephys/26.2.179, 2006.
729 Fang, Y. L., Leung, L. R., Knox, R., Koven, C., and Bond-Lamberty, B.: Impact of the numerical
730 solution approach of a plant hydrodynamic model (v0.1) on vegetation dynamics, Geosci Model
731 Dev, 15, 6385-6398, 10.5194/gmd-15-6385-2022, 2022.
732 Fisher, R., McDowell, N., Purves, D., Moorcroft, P., Sitch, S., Cox, P., Huntingford, C., Meir, P.,
733 and Woodward, F. I.: Assessing uncertainties in a second-generation dynamic vegetation model
734 caused by ecological scale limitations, New Phytol, 187, 666-681, 10.1111/j.1469-
735 8137.2010.03340.x, 2010.
736 Fisher, R. A. and Koven, C. D.: Perspectives on the Future of Land Surface Models and the
737 Challenges of Representing Complex Terrestrial Systems, J Adv Model Earth Sy, 12, ARTN
738 e2018MS001453: 10.1029/2018MS001453, 2020.
739 Fisher, R. A., Muszala, S., Verteinstein, M., Lawrence, P., Xu, C., McDowell, N. G., Knox, R.
740 G., Koven, C., Holm, J., Rogers, B. M., Spessa, A., Lawrence, D., and Bonan, G.: Taking off the
741 training wheels: the properties of a dynamic vegetation model without climate envelopes,
742 CLM4.5(ED), Geosci Model Dev, 8, 3593-3619, 10.5194/gmd-8-3593-2015, 2015.
743 Fisher, R. A., Koven, C. D., Anderegg, W. R. L., Christoffersen, B. O., Dietze, M. C., Farrior, C.
744 E., Holm, J. A., Hurtt, G. C., Knox, R. G., Lawrence, P. J., Lichstein, J. W., Longo, M.,
745 Matheny, A. M., Medvigy, D., Muller-Landau, H. C., Powell, T. L., Serbin, S. P., Sato, H.,
746 Shuman, J. K., Smith, B., Trugman, A. T., Viskari, T., Verbeeck, H., Weng, E. S., Xu, C. G., Xu,
747 X. T., Zhang, T., and Moorcroft, P. R.: Vegetation demographics in Earth System Models: A
748 review of progress and priorities, Global Change Biol, 24, 35-54, 10.1111/gcb.13910, 2018.
749 Gleason, S. M., Westoby, M., Jansen, S., Choat, B., Hacke, U. G., Pratt, R. B., Bhaskar, R.,
750 Brodribb, T. J., Bucci, S. J., Cao, K. F., Cochard, H., Delzon, S., Domec, J. C., Fan, Z. X., Feild,
751 T. S., Jacobsen, A. L., Johnson, D. M., Lens, F., Maherali, H., Martinez-Vilalta, J., Mayr, S.,
752 McCulloh, K. A., Mencuccini, M., Mitchell, P. J., Morris, H., Nardini, A., Pittermann, J.,
753 Plavcova, L., Schreiber, S. G., Sperry, J. S., Wright, I. J., and Zanne, A. E.: Weak tradeoff
754 between xylem safety and xylem-specific hydraulic efficiency across the world's woody plant
755 species, New Phytol, 209, 123-136, 10.1111/nph.13646, 2016.
756 Hammond, W. M., Yu, K., Wilson, L. A., Will, R. E., Anderegg, W. R. L., and Adams, H. D.:
757 Dead or dying? Quantifying the point of no return from hydraulic failure in drought-induced tree
758 mortality, New Phytol, 223, 1834-1843, https://doi.org/10.1111/nph.15922, 2019.
759 Hochberg, U., Rockwell, F. E., Holbrook, N. M., and Cochard, H.: Iso/Anisohydry: A Plant-
760 Environment Interaction Rather Than a Simple Hydraulic Trait, Trends Plant Sci, 23, 112-120,
761 10.1016/j.tplants.2017.11.002, 2018.
762 Huang, M. Y., Xu, Y., Longo, M., Keller, M., Knox, R. G., Koven, C. D., and Fisher, R. A.:
763 Assessing impacts of selective logging on water, energy, and carbon budgets and ecosystem
764 dynamics in Amazon forests using the Functionally Assembled Terrestrial Ecosystem Simulator,
765 Biogeosciences, 17, 4999-5023, 10.5194/bg-17-4999-2020, 2020.
766 Iversen, C. M., McCormack, M. L., Powell, A. S., Blackwood, C. B., Freschet, G. T., Kattge, J.,
767 Roumet, C., Stover, D. B., Soudzilovskaia, N. A., Valverde-Barrantes, O. J., van Bodegom, P.
768 M., and Violle, C.: A global Fine-Root Ecology Database to address below-ground challenges in
769 plant ecology, New Phytol, 215, 15-26, 10.1111/nph.14486, 2017.

Kennedy, D., Swenson, S., Oleson, K. W., Lawrence, D. M., Fisher, R., da Costa, A. C. L., and Gentine, P.: Implementing Plant Hydraulics in the Community Land Model, Version 5, J Adv Model Earth Sy, 11, 485-513, 10.1029/2018ms001500, 2019.

Klein, T.: The variability of stomatal sensitivity to leaf water potential across tree species indicates a continuum between isohydric and anisohydric behaviours, Funct Ecol, 28, 1313-1320, 10.1111/1365-2435.12289, 2014.

Koven, C. D., Knox, R. G., Fisher, R. A., Chambers, J. Q., Christoffersen, B. O., Davies, S. J., Detto, M., Dietze, M. C., Faybishenko, B., Holm, J., Huang, M. Y., Kovenock, M., Kueppers, L. M., Lemieux, G., Massoud, E., McDowel, N. G., Muller-Landau, H. C., Needham, J. F., Norby, R. J., Powell, T., Rogers, A., Serbin, S. P., Shuman, J. K., Swann, A. L. S., Varadharajan, C., Walker, A. P., Wright, S. J., and Xu, C. G.: Benchmarking and parameter sensitivity of physiological and vegetation dynamics using the Functionally Assembled Terrestrial Ecosystem Simulator (FATES) at Barro Colorado Island, Panama, Biogeosciences, 17, 3017-3044, 10.5194/bg-17-3017-2020, 2020.

Kunert, N., Zailaa, J., Herrmann, V., Muller-Landau, H. C., Wright, S. J., Perez, R., McMahon, S. M., Condit, R. C., Hubbell, S. P., Sack, L., Davies, S. J., and Anderson-Teixeira, K. J.: Leaf turgor loss point shapes local and regional distributions of evergreen but not deciduous tropical trees, New Phytol, 230, 485-496, 10.1111/nph.17187, 2021.

Kursar, T. A., Engelbrecht, B. M. J., Burke, A., Tyree, M. T., El Omari, B., and Giraldo, J. P.: Tolerance to low leaf water status of tropical tree seedlings is related to drought performance and distribution, Funct Ecol, 23, 93-102, 10.1111/j.1365-2435.2008.01483.x, 2009.

Lambert, M. S. A., Tang, H., Aas, K. S., Stordal, F., Fisher, R. A., Fang, Y. L., Ding, J. Y., and Parmentier, F. J. W.: Inclusion of a cold hardening scheme to represent frost tolerance is essential to model realistic plant hydraulics in the Arctic-boreal zone in CLM5.0-FATES-Hydro, Geosci Model Dev, 15, 8809-8829, 10.5194/gmd-15-8809-2022, 2022.

Lawrence, D. M., Fisher, R. A., Koven, C. D., Oleson, K. W., Swenson, S. C., Bonan, G., Collier, N., Ghimire, B., van Kampenhout, L., Kennedy, D., Kluzek, E., Lawrence, P. J., Li, F., Li, H. Y., Lombardozzi, D., Riley, W. J., Sacks, W. J., Shi, M. J., Vertenstein, M., Wieder, W. R., Xu, C. G., Ali, A. A., Badger, A. M., Bisht, G., van den Broeke, M., Brunke, M. A., Burns, S. P., Buzan, J., Clark, M., Craig, A., Dahlin, K., Drewniak, B., Fisher, J. B., Flanner, M., Fox, A. M., Gentine, P., Hoffman, F., Keppel-Aleks, G., Knox, R., Kumar, S., Lenaerts, J., Leung, L. R., Lipscomb, W. H., Lu, Y. Q., Pandey, A., Pelletier, J. D., Perket, J., Randerson, J. T., Ricciuto, D. M., Sanderson, B. M., Slater, A., Subin, Z. M., Tang, J. Y., Thomas, R. Q., Martin, M. V., and Zeng, X. B.: The Community Land Model Version 5: Description of New Features, Benchmarking, and Impact of Forcing Uncertainty, J Adv Model Earth Sy, 11, 4245-4287, 10.1029/2018ms001583, 2019.

Manzoni, S., Vico, G., Katul, G., Palmroth, S., Jackson, R. B., and Porporato, A.: Hydraulic limits on maximum plant transpiration and the emergence of the safety-efficiency trade-off, New Phytol, 198, 169-178, 10.1111/nph.12126, 2013.

Massoud, E. C., Xu, C. G., Fisher, R. A., Knox, R. G., Walker, A. P., Serbin, S. P., Christoffersen, B. O., Holm, J. A., Kueppers, L. M., Ricciuto, D. M., Wei, L., Johnson, D. J., Chambers, J. Q., Koven, C. D., McDowell, N. G., and Vrugt, J. A.: Identification of key parameters controlling demographically structured vegetation dynamics in a land surface model: CLM4.5(FATES), Geosci Model Dev, 12, 4133-4164, 10.5194/gmd-12-4133-2019, 2019.

McDowell, N., Allen, C. D., Anderson-Teixeira, K., Brando, P., Brienen, R., Chambers, J., Christoffersen, B., Davies, S., Doughty, C., Duque, A., Espirito-Santo, F., Fisher, R., Fontes, C.

816 G., Galbraith, D., Goodsman, D., Grossiord, C., Hartmann, H., Holm, J., Johnson, D. J., Kassim,
817 A., Keller, M., Koven, C., Kueppers, L., Kumagai, T., Malhi, Y., McMahon, S. M., Mencuccini,
818 M., Meir, P., Moorcroft, P., Muller-Landau, H. C., Phillips, O. L., Powell, T., Sierra, C. A.,
819 Sperry, J., Warren, J., Xu, C. G., and Xu, X. T.: Drivers and mechanisms of tree mortality in
820 moist tropical forests, New Phytol, 219, 851-869, 10.1111/nph.15027, 2018.
821 McDowell, N. G., Fisher, R. A., Xu, C. G., Domec, J. C., Holtta, T., Mackay, D. S., Sperry, J. S.,
822 Boutz, A., Dickman, L., Gehres, N., Limousin, J. M., Macalady, A., Martinez-Vilalta, J.,
823 Mencuccini, M., Plaut, J. A., Ogee, J., Pangle, R. E., Rasse, D. P., Ryan, M. G., Sevanto, S.,
824 Waring, R. H., Williams, A. P., Yepez, E. A., and Pockman, W. T.: Evaluating theories of
825 drought-induced vegetation mortality using a multimodel-experiment framework, New Phytol,
826 200, 304-321, 10.1111/nph.12465, 2013.
827 McDowell, N. G., Sapes, G., Pivovaroff, A., Adams, H. D., Allen, C. D., Anderegg, W. R. L.,
828 Arend, M., Breshears, D. D., Brodribb, T., Choat, B., Cochard, H., De Caceres, M., De Kauwe,
829 M. G., Grossiord, C., Hammond, W. M., Hartmann, H., Hoch, G., Kahmen, A., Klein, T.,
830 Mackay, D. S., Mantova, M., Martinez-Vilalta, J., Medlyn, B. E., Mencuccini, M., Nardini, A.,
831 Oliveira, R. S., Sala, A., Tissue, D. T., Torres-Ruiz, J. M., Trowbridge, A. M., Trugman, A. T.,
832 Wiley, E., and Xu, C. G.: Mechanisms of woody-plant mortality under rising drought, CO2 and
833 vapour pressure deficit, Nat Rev Earth Env, 3, 294-308, 10.1038/s43017-022-00272-1, 2022.
834 Moorcroft, P. R., Hurtt, G. C., and Pacala, S. W.: A method for scaling vegetation dynamics: The
835 ecosystem demography model (ED), Ecol Monogr, 71, 557-585, 10.1890/0012-
836 9615(2001)071[0557:Amfsvd]2.0.Co;2, 2001.
837 Needham, J. F., Chambers, J., Fisher, R., Knox, R., and Koven, C. D.: Forest responses to
838 simulated elevated CO2 under alternate hypotheses of size- and age-dependent mortality, Global
839 Change Biol, 26, 5734-5753, 10.1111/gcb.15254, 2020.
840 Norman, J.: Modelling the complete crop canopy, in Modification of the Aerial Environment of
841 Plants, Am. Soc. Agri. Eng. Monograph, 2, 249-277, 1979.
842 North, G. B. and Nobel, P. S.: Drought-Induced Changes in Hydraulic Conductivity and
843 Structure in Roots of Ferocactus-Acanthodes and Opuntia-Ficus-Indica, New Phytol, 120, 9-19,
844 DOI 10.1111/j.1469-8137.1992.tb01053.x, 1992.
845 Oleson, K. W., Lawrence, D. M., Bonan, G. B., Drewniak, B., Huang, M., Koven, C. D., Levis,
846 S., Li, F., Riley, W. J., Subin, Z. M., Swenson, S. C., Thornton, P. E., Bozbiyik, A., Fisher, R.,
847 Heald, C. L., Kluzek, E., Lamarque, J.-F., Lawrence, P. J., Leung, L. R., Lipscomb, W.,
848 Muszala, S., Ricciuto, D. M., Sacks, W., Sun, Y., Tang, J., & Yang, Z.-L. : Technical description
849 of version 4.5 of the Community Land Model (CLM) National Center for Atmospheric Research,
850 Boulder, Colorado, USA.Tech. Rep. NCAR/TN-503+STR, 2013.
851 Olson, M. E., Anfodillo, T., Gleason, S. M., and McCulloh, K. A.: Tip-to-base xylem conduit
852 widening as an adaptation: causes, consequences, and empirical priorities, New Phytol, 229,
853 1877-1893, 10.1111/nph.16961, 2021.
854 Paton, S.: Yearly Reports_Barro Colorado Island, Smithsonian Tropical Research Institute,
855 https://doi.org/10.25573/data.11799111.v3, 2020.
856 Pineda-Garcia, F., Paz, H., and Meinzer, F. C.: Drought resistance in early and late secondary
857 successional species from a tropical dry forest: the interplay between xylem resistance to
858 embolism, sapwood water storage and leaf shedding, Plant Cell Environ, 36, 405-418,
859 10.1111/j.1365-3040.2012.02582.x, 2013.

Poudel, M., Mendes, R., Costa, L. A., Bueno, C. G., Meng, Y., Folimonova, S. Y., Garrett, K. A., and Martins, S. J.: The role of plant-associated bacteria, fungi, and viruses in drought stress mitigation, Frontiers in microbiology, 12, 3058, 2021.

Powell, T. L., Wheeler, J. K., de Oliveira, A. A. R., da Costa, A. C. L., Saleska, S. R., Meir, P., and Moorcroft, P. R.: Differences in xylem and leaf hydraulic traits explain differences in drought tolerance among mature Amazon rainforest trees, Global Change Biol, 23, 4280-4293, 10.1111/gcb.13731, 2017.

Powell, T. L., Koven, C. D., Johnson, D. J., Faybishenko, B., Fisher, R. A., Knox, R. G., McDowell, N. G., Condit, R., Hubbell, S. P., Wright, S. J., Chambers, J. Q., and Kueppers, L. M.: Variation in hydroclimate sustains tropical forest biomass and promotes functional diversity, New Phytol, 219, 932-946, 10.1111/nph.15271, 2018.

Roderick, M. L., Berry, S. L., Saunders, A. R., and Noble, I. R.: On the relationship between the composition, morphology and function of leaves, Funct Ecol, 13, 696-710, DOI 10.1046/j.1365-2435.1999.00369.x, 1999.

Rodriguez-Zaccaro, F. D., Valdovinos-Ayala, J., Percolla, M. I., Venturas, M. D., Pratt, R. B., and Jacobsen, A. L.: Wood structure and function change with maturity: Age of the vascular cambium is associated with xylem changes in current-year growth, Plant, Cell & Environment, 42, 1816-1831, https://doi.org/10.1111/pce.13528, 2019.

Rowland, L., da Costa, A. C. L., Galbraith, D. R., Oliveira, R. S., Binks, O. J., Oliveira, A. A. R., Pullen, A. M., Doughty, C. E., Metcalfe, D. B., Vasconcelos, S. S., Ferreira, L. V., Malhi, Y., Grace, J., Mencuccini, M., and Meir, P.: Death from drought in tropical forests is triggered by hydraulics not carbon starvation, Nature, 528, 119-+, 10.1038/nature15539, 2015.

Sack, L., Cowan, P. D., Jaikumar, N., and Holbrook, N. M.: The 'hydrology' of leaves: co-ordination of structure and function in temperate woody species, Plant Cell Environ, 26, 1343-1356, DOI 10.1046/j.0016-8025.2003.01058.x, 2003.

Savage, V. M., Bentley, L. P., Enquist, B. J., Sperry, J. S., Smith, D. D., Reich, P. B., and von Allmen, E. I.: Hydraulic trade-offs and space filling enable better predictions of vascular structure and function in plants, P Natl Acad Sci USA, 107, 22722-22727, 10.1073/pnas.1012194108, 2010.

Schmidhalter, U.: The gradient between pre-dawn rhizoplane and bulk soil matric potentials, and its relation to the pre-dawn root and leaf water potentials of four species, Plant, Cell & Environment, 20, 953-960, https://doi.org/10.1046/j.1365-3040.1997.d01-136.x, 1997.

Seneviratne, S. I., Zhang, X., Adnan, M., Badi, W., Dereczynski, C., Luca, A. D., Ghosh, S., Iskandar, I., Kossin, J., Lewis, S., Otto, F., Pinto, I., Satoh, M., Vicente-Serrano, S. M., Wehner, M., Zhou, B., and Allan, R.: Weather and climate extreme events in a changing climate, in: Climate Change 2021: The Physical Science Basis: Working Group I contribution to the Sixth Assessment Report of the Intergovernmental Panel on Climate Change, edited by: Masson-Delmotte, V. P., Zhai, A., Pirani, S. L., and Connors, C., Cambridge University Press, Cambridge, UK, 1513-1766, 2021.

Shinozaki, K., Yoda, K., Hozumi, K., and Kira, T.: A quantitative analysis of plant form-the pipe model theory: I. Basic analyses, Japanese Journal of ecology, 14, 97-105, 1964.

Slot, M., Nardwattanawong, T., Hernandez, G. G., Bueno, A., Riederer, M., and Winter, K.: Large differences in leaf cuticle conductance and its temperature response among 24 tropical tree species from across a rainfall gradient, New Phytol, 232, 1618-1631, 10.1111/nph.17626, 2021.

Smith, D. D., Sperry, J. S., Enquist, B. J., Savage, V. M., McCulloh, K. A., and Bentley, L. P.: Deviation from symmetrically self-similar branching in trees predicts altered hydraulics,

906 mechanics, light interception and metabolic scaling, New Phytol, 201, 217-229,
907 10.1111/nph.12487, 2014.
908 Sperry, J. S. and Love, D. M.: What plant hydraulics can tell us about responses to climate-
909 change droughts, New Phytol, 207, 14-27, 10.1111/nph.13354, 2015.
910 Su, R., Liu, H., Wang, C., Zhang, H., and Cui, J.: Leaf turgor loss point is one of the best
911 predictors of drought-induced tree mortality in tropical forest, Front Ecol Evol, 10, ARTN
912 974004: 10.3389/fevo.2022.974004, 2022.
913 Tyree, M. T. and Yang, S.: Water-storage capacity of Thuja, Tsuga and Acer stems measured by
914 dehydration isotherms: the contribution of capillary water and cavitation, Planta, 182, 420-426,
915 1990.
916 Wei, L., Xu, C. G., Jansen, S., Zhou, H., Christoffersen, B. O., Pockman, W. T., Middleton, R.
917 S., Marshall, J. D., and McDowell, N. G.: A heuristic classification of woody plants based on
918 contrasting shade and drought strategies, Tree Physiol, 39, 767-781, 10.1093/treephys/tpy146,
919 2019.
920 Wolfe, B. T.: Bark water vapour conductance is associated with drought performance in tropical
921 trees, Biol Letters, 16, ARTN 20200263: 10.1098/rsbl.2020.0263, 2020.
922 Wright, S. J., Kitajima, K., Kraft, N. J. B., Reich, P. B., Wright, I. J., Bunker, D. E., Condit, R.,
923 Dalling, J. W., Davies, S. J., Diaz, S., Engelbrecht, B. M. J., Harms, K. E., Hubbell, S. P., Marks,
924 C. O., Ruiz-Jaen, M. C., Salvador, C. M., and Zanne, A. E.: Functional traits and the growth-
925 mortality trade-off in tropical trees, Ecology, 91, 3664-3674, Doi 10.1890/09-2335.1, 2010.
926 Xu, C. G. and Gertner, G.: Understanding and comparisons of different sampling approaches for
927 the Fourier Amplitudes Sensitivity Test (FAST), Comput Stat Data An, 55, 184-198,
928 10.1016/j.csda.2010.06.028, 2011a.
929 Xu, C. G. and Gertner, G. Z.: Reliability of global sensitivity indices, J Stat Comput Sim, 81,
930 1939-1969, 10.1080/00949655.2010.509317, 2011b.
931 Xu, C. G., McDowell, N. G., Fisher, R. A., Wei, L., Sevanto, S., Christoffersen, B. O., Weng, E.
932 S., and Middleton, R. S.: Increasing impacts of extreme droughts on vegetation productivity
933 under climate change, Nat Clim Change, 9, 948-+, 10.1038/s41558-019-0630-6, 2019.
934 Xu, X. T., Medvigy, D., Powers, J. S., Becknell, J. M., and Guan, K. Y.: Diversity in plant
935 hydraulic traits explains seasonal and inter-annual variations of vegetation dynamics in
936 seasonally dry tropical forests, New Phytol, 212, 80-95, 10.1111/nph.14009, 2016.
937 Yang, S. D. and Tyree, M. T.: Hydraulic Resistance in Acer-Saccharum Shoots and Its Influence
938 on Leaf Water Potential and Transpiration, Tree Physiol, 12, 231-242, DOI
939 10.1093/treephys/12.3.231, 1993.
940